

**FUNWAVE-TVD**  
FULLY NONLINEAR BOUSSINESQ WAVE MODEL  
WITH TVD SOLVER  
DOCUMENTATION AND USER'S MANUAL  
**(VERSION 2.1)**

FENGYAN SHI, BABAK TEHRANIRAD AND JAMES T. KIRBY  
CENTER FOR APPLIED COASTAL RESEARCH, UNIVERSITY OF  
DELAWARE, NEWARK, DE 19716

JEFFREY C. HARRIS AND STEPHAN GRILLI  
DEPARTMENT OF OCEAN ENGINEERING, UNIVERSITY OF  
RHODE ISLAND, NARRAGANSETT, RI 02882

RESEARCH REPORT NO. CACR-11-04  
SEPTEMBER, 2013



**CENTER FOR APPLIED COASTAL RESEARCH**  
Ocean Engineering Laboratory  
University of Delaware  
Newark, Delaware 19716

## **Acknowledgements**

This model development was a part of the surfzone optics project sponsored by the Office of Naval Research, Coastal Geosciences Program through grant N00014-10-1-0088.

## **Abstract**

The report documents a new version of the fully nonlinear Boussinesq wave model (FUN-WAVE) initially developed by Kirby et al. (1998). The development of the present version was motivated by recent needs for modeling of surfzone-scale optical properties in a Boussinesq model framework, and modeling of Tsunami wave in both a regional/coastal scale for prediction of coastal inundation and a basin scale for wave propagation. This version features several theoretical and numerical improvements, including 1) a more complete set of fully nonlinear Boussinesq equations; 2) MUSCL-TVD solver with adaptive Runge-Kutta time stepping; 3) Shock-capturing wave breaking scheme; 4) wetting-drying moving boundary condition with incorporation of HLL construction method into the scheme; 5) an option for parallel computation. The documentation provides derivations of the conservation form of theoretical equations, re-arrangement of pressure gradient term in order to obtain a numerically well-balanced form, detailed numerical schemes, users' manual and examples. Users can also refer to Shi et al. (2012a) for the Cartesian version and Kirby et al. (2012) for the spherical version of the model.

The present version (Version 2.1) has been fully tested using the existing examples in the previous report (Shi et al., 2011) and tsunami benchmark tests in spherical coordinates reported by Tehranirad et al. (2013).

# Contents

<b>Differences between Version 1.1 and Version 1.0</b>	<b>8</b>
<b>Differences between Version 2.0 and Version 1.1</b>	<b>8</b>
<b>Differences between Version 2.1 and Version 2.0</b>	<b>9</b>
<b>1 Introduction</b>	<b>10</b>
<b>2 Theory</b>	<b>13</b>
2.1 Governing equations . . . . .	13
2.2 Treatment of the surface gradient term . . . . .	15
2.3 Conservative form of fully nonlinear Boussinesq equations . . . . .	16
<b>3 Numerical schemes</b>	<b>17</b>
3.1 Compact form of governing equations . . . . .	17
3.2 Spatial discretization . . . . .	18
3.3 Time stepping . . . . .	20
3.4 Wave breaking and wetting-drying schemes for shallow water . . . . .	20
3.5 Boundary conditions, wavemaker and wind effect . . . . .	21
3.6 Parallelization . . . . .	21
3.7 Implementation of weakly nonlinear Boussinesq equations in spherical coordinates	21
<b>4 Users' Manual</b>	<b>26</b>
4.1 Program outline and flow chart . . . . .	26
4.2 Subroutine and function descriptions . . . . .	26
4.3 Permanent variables . . . . .	31
4.4 Installation and compilation . . . . .	34
4.5 Input . . . . .	34
4.5.1 Specifications of Grid Inputs . . . . .	41
4.6 Input for the spherical code . . . . .	41
4.7 Model nesting . . . . .	42
4.8 Output . . . . .	43
<b>5 Examples</b>	<b>43</b>
5.1 Breaking waves on a beach . . . . .	44
5.2 Random wave shoaling and breaking on a slope (in directory /mase_kirby_1d/) . .	46
5.3 Wave propagation over a shoal: Berkhoff et al. (1982) (in directory /berkhoff_2d/)	53
5.4 Solitary wave on a conical island . . . . .	57
5.5 Solitary wave runup on a shelf with an island (in directory /solitary_runup_2d) . . .	62
5.6 Nesting case . . . . .	69

## List of Figures

1	Variation in model performance with number of processors for a 1800 x 1800 domain. Straight line indicates arithmetic speedup. Actual performance is shown in the curved line. . . . .	22
2	Flow chart of the main program. . . . .	27
3	Comparisons of wave height (upper panel) and wave setup (lower panel) between measured data and model results from grid resolutions of $dx = 0.0125$ m, $0.025$ m and $0.050$ m, respectively. Case: plunging breaker. . . . .	46
4	Snapshots of surface elevation at $t = 17.4$ , $18.6$ and $19.9$ s from models with grid resolutions of $dx = 0.025$ (solid lines) and $0.050$ m (dashed lines). . . . .	47
5	Model/data comparisons of wave height (upper panel) and wave setup ( $dx = 0.025$ m). Case: spilling breaker. . . . .	48
6	Experiment layout of Mase and Kirby (1992). . . . .	50
7	Time series comparison of $\eta$ between model (dashed lines) and data (solid lines) at 11 wave gauges in Mase and Kirby (1992). . . . .	50
8	Comparison of skewness ( $\circ$ ) and asymmetry ( $\times$ ) at different water depths. Solid lines are experiment data ( Mase and Kirby, 1992). Dashed lines are numerical results	51
9	Experiment layout for wave focusing experiment of Berkhoff et al. (1982). . . . .	54
10	Comparisons of wave height along specified sections between the model (solid lines) and experiment data (circles). . . . .	55
11	View of conical island(top) and basin(bottom)(from Synolakis et al (2007, Figure A16)). . . . .	58
12	Definition sketch for conical island. All dimensions are in cm (from Synolakis et al (2007, Figure A17)). . . . .	58
13	Schematic gauge locations around the conical island(from Synolakis et al (2007, Figure A18)). . . . .	59
14	Comparison of computed and measured time series of free surface for $H/d = 0.045$ .Solid lines: measured, Dashed lines: Computed. . . . .	60
15	Comparison of computed and measured time series of free surface for $H/d = 0.091$ .Solid lines: measured, Dashed lines: Computed. . . . .	61
16	Comparison of computed and measured time series of free surface for $H/d = 0.181$ .Solid lines: measured, Dashed lines: Computed. . . . .	61
17	Bathymetry contours (in meters) and measurement locations used in model/data comparisons. Circles: pressure gauges, triangles: ADV. . . . .	63
18	Modeled water surface at (top) $t = 6.4$ s, (middle) $t = 8.4$ s, (bottom) $t = 14.4$ s. . . .	64
19	Time step variation. . . . .	65
20	Model/data comparisons of time series of surface elevation at (top) Gauge 1 - Gauge 9. Solid line: model, stars: data. . . . .	66

21	Model/data comparisons of time series of velocity $u$ component at ADV 1 (top panel), ADV 2 (second panel), ADV 3 (third panel), and $v$ component at ADV 3 (bottom panel). Solid line: model, dashed line: data. . . . .	67
22	Solitary wave calculated in a larger domain Grid_A (upper) and in a nested smaller domain Grid_B (lower) at $t=100s, 200s, 300s,$ and $400s.$ . . . . .	73

**List of Tables**

1    Percent error of predicted maximum runup calculated for each gauge in conical island test. . . . . 59

## Differences between Version 1.1 and Version 1.0

The major updates from FUNWAVE-TVD Version 1.0 to Version 1.1 are new model capabilities in grid nesting, incorporation of wind effect, wave generation in the spherical mode and calculation of time-averaged properties. Version 1.1 has been fully tested using the existing examples in the previous report for Version 1.0 and tsunami benchmark tests in spherical coordinates reported by Shi et al. (2012b). Detailed updates are listed below.

1. One-way grid nesting capability was added in Version 1.1 (subroutine `OneWayCoupling`). The nesting schemes and an example are shown in section 4 and section 5, respectively.
2. Wind effect was added based on Chen et al. (2004). Users should specify `-DWIND` in Makefile in order to use this option. Details are described in section 4.5.
3. Output of mean velocities.
4. Wavemakers were added in the spherical mode in order to conduct benchmark tests (Shi et al., 2012b).
5. Coding for `VANLEER_LIMITER ()` was modified for a better computational efficiency.
6. At a wet-dry interface, water depth at cell interface (`DepthX` and `DepthY`) was evaluated using the depth at the cell center of the wet point. This approach can avoid an extreme large value of slope caused by the raw topographic data (e.g., NGDC data).
7. Bugs were fixed for `MASK9` where the previously defined array has a different size from that of `U` and `V`.

## Differences between Version 2.0 and Version 1.1

The major change from Version 1.1 to Version 2.0 is for the spherical mode. Recently, Kirby et al. (2012) formulated a more complete set of Boussinesq equations in spherical coordinates. The equations include both weakly nonlinear and fully nonlinear forms based on velocities at a reference level  $z_\alpha$ . In version 2.0, we implemented the weakly nonlinear formulations. Version 2.0 has been fully tested using the existing examples in the previous report for Version 1.0/1.1 and tsunami benchmark tests in spherical coordinates (Shi et al., 2012). Other updates are listed below.

1. Compared to Version 1.1, a more accurate scheme for grid nesting was implemented. Affected subroutines include `PHI_COLL`, `CAL_DISPERSION` and `GET_Eta_U_V_HU_HV`. Boundary conditions for dispersion terms were removed at nesting boundaries (in `PHI_COLL` and `CAL_DISPERSION`). Boundary conditions at nesting boundaries are added in the tridiagonal solver (`GET_Eta_U_V_HU_HV`). To activate this option, set `-DZALPHA` in Makefile.
2. The wall clock was added in the main program.

3. Input format for gauges was changed to geographic coordinates (Lat/Lon) in the spherical mode (Version 1.1 and earlier used grid numbers I and J).
4. Several useless subroutines were removed from the code.

## **Differences between Version 2.1 and Version 2.0**

The major change from Version 2.0 to Version 2.1 is for the friction factor specifications. Inside previous versions the model used a fixed friction factor for the whole modeling domain. However, in version 2.1 the model is capable of reading an initial friction field (friction coefficient matrix) that can be defined differently for each grid by the user. Also, the code is now able to use Manning coefficient as well as conventional friction factor. Moreover, output system efficiency is upgraded inside version 2.1 and several variable are added to the recording list of FUNWAVE-TVD. Updates are listed below.

1. Version 2.1 is capable of reading an input file for friction coefficient for cases in which friction field is not homogeneous.
2. Version 2.1 is able to use Manning coefficient formulation (in addition to friction coefficient formulation) to calculate friction force. To activate this option, set -DMANNING in Makefile.
3. The efficiency of writing the output files is upgraded in this version.
4. In version 2.1, user can print the maximum momentum flux, maximum velocity, and minimum surface elevation as well as maximum vorticity in addition to other output variable in prior versions.

# 1 Introduction

Boussinesq wave models have become a useful tool for modeling surface wave transformation from deep water to the swash zone, as well as wave-induced circulation inside the surfzone. Improvements in the range of model applicability have been obtained with respect to classical restrictions to both weak dispersion and weak nonlinearity. Madsen et al (1991) and Nwogu (1993) demonstrated that the order of approximation in reproducing frequency dispersion effects could be increased using either judicious choices for the form (or reference point) for Taylor series expansions for the vertical structure of dependent variables, or operators effecting a rearrangement of dispersive terms in already-developed model equations. These approaches, combined with use either of progressively higher order truncated series expansions (Gobbi et al, 2000; Agnon et al, 1999) or multiple level representations (Lynett and Liu, 2004), have effectively eliminated the restriction of this class of model to relatively shallow water, allowing for their application to the entire shoaling zone or deeper. At the same time, the use of so-called "fully-nonlinear" formulations (e.g., Wei et al (1995) and many others) effectively eliminates the restriction to weak nonlinearity by removing the wave height to water depth ratio as a scaling or expansion parameter in the development of approximate governing equations. This approach has improved model applicability in the surf and swash zones particularly, where surface fluctuations are of the order of mean water depth at least and which can represent the total vertical extent of the water column in swash conditions. Representations of dissipative wave-breaking events, which do not naturally arise as weak discontinuous solutions in the dispersive Boussinesq formulation, have been developed usually following an eddy viscosity formulation due to Zelt (1991), and have been shown to be highly effective in describing surf zone wave height decay. The resulting class of models has been shown to be highly effective in modeling wave-averaged surf zone flows over both simple (Chen et al, 2003; Feddersen et al, 2011) and complex (Geiman et al, 2011) bathymetries. Kim et al (2009) have further extended the formulation to incorporate a consistent representation of boundary layer turbulence effects on vertical flow structure.

Existing approaches to development of numerical implementations for Boussinesq models include a wide range of finite difference, finite volume, or finite element formulations. In this paper, we describe the development of a new numerical approach for the FUNWAVE model (Kirby et al, 1998), which has been widely used as a public domain open-source code since it's initial development. FUNWAVE was originally developed using an unstaggered finite difference formulation for spatial derivatives together with an iterated 4th order Adams-Bashforth-Moulton (ABM) scheme for time stepping (Wei and Kirby, 1995), applied to the fully nonlinear model equations of Wei et al (1995). In this scheme, spatial differencing is handled using a mixed-order approach, employing fourth-order accurate centered differences for first derivatives and second-order accurate differences for third derivatives. This choice was made in order to move leading order truncation errors to one order higher than the  $O(\mu^2)$  dispersive terms (where  $\mu$  is ratio of a characteristic water depth to a horizontal length, a dimensionless parameter characterizing frequency dispersion), while maintaining the tridiagonal structure of spatial derivatives within time-derivative terms. This scheme is straightforward to develop and has been widely utilized in other Boussinesq models.

Kennedy et al (2000) and Chen et al (2000) describe further aspects of the model system aimed at generalizing it for use in modeling surf zone flows. Breaking is handled using a generalization to two horizontal dimensions of the eddy viscosity model of Zelt (1991). Similar approaches have been used by other Boussinesq model developers, such as Nwogu and Demirbilek (2001), who used a more sophisticated eddy viscosity model in which the eddy viscosity is expressed in terms of turbulent kinetic energy and a length scale. The presence of a moving shoreline in the swash zone is handled using a “slot” or porous-beach method, in which the entire domain remains wetted using a network of slots at grid resolution which are narrow but which extend down to a depth lower than the minimum expected excursion of the modelled free surface. These generalizations form the basis for the existing public domain version of the code (Kirby et al, 1998). Subsequently, several extensions have been made in research versions of the code. Kennedy et al (2001) improved nonlinear performance of the model by utilizing an adaptive reference level for vertical series expansions, which is allowed to move up and down with local surface fluctuations. Chen et al (2003) extended the model to include longshore periodic boundary conditions and described its application to modeling longshore currents on relatively straight coastlines. Shi et al (2001) generalized the model coordinate system to non-orthogonal curvilinear coordinates. Finally, Chen et al (2003) and Chen (2006) provided revised model equations which correct deficiencies in the representation of higher order advection terms, leading to a set of model equations which, in the absence of dissipation effects, conserve depth-integrated potential vorticity to  $O(\mu^2)$ , consistent with the level of approximation in the model equations.

The need for a new formulation for FUNWAVE arose from recognition of several crucial problems with the existing code. First, the original model proved to be “noisy”, or at least weakly unstable to high wavenumbers near the grid Nyquist limit. In addition, both the implementation of the eddy viscosity model for surf zone wave breaking and the interaction of runup with beach slots proved to be additional sources of noise in model calculations. In the original unstaggered grid finite difference scheme, these effects led to the need for periodic application of dissipative filters, with the frequency of filtering increased in areas with active breaking. The overall grid-based noise generation was found to stem from several sources. First, Kennedy (2001, personal communications), during development of a High Performance Fortran (HPF) version of the code on an early linux cluster, discovered that the noise was partially due to implementation of boundary conditions and could be alleviated to an extent. At the same time, the curvilinear model developed by Shi et al (2001) was implemented using a staggered grid for spatial differencing, and the resulting code was found to be less susceptible to the general grid noise problem. A comparison of noise levels in the original FUNWAVE, the staggered grid scheme of Shi et al, and the corrected boundary condition formulation of Kennedy may be found in Zhen (2004).

Additional sources of noise related either to the eddy viscosity formulation or interaction between the flow and beach “slots” remain less well analyzed or understood. In addition, the performance of the slots themselves has been called into question in several cases involving inundation over complex bathymetry. Slots which are too wide relative to the model grid spacing may admit too much fluid before filling during runup, and cause both a reduction in amplitude and a phase lag in modeled runup events. At the other extreme, slots which are too narrow tend to induce a

great deal of numerical noise, leading to the need for intermittent or even fairly frequent filtering of swash zone solutions. Poor model performance in comparison to data for the case of Swigler and Lynett (2011), described below in section 4.3, was the determining factor in the decision to pursue a new model formulation.

A number of recently development Boussinesq-type wave models have used a hybrid method combining the finite-volume and finite-difference TVD (Total Variation Diminishing)-type schemes (Toro, 2009), and have shown robust performance of the shock-capturing method in simulating breaking waves and coastal inundation (Tonelli and Petti, 2009, 2010, Roeber et al., 2010, Shiach and Mingham, 2009, Erduran et al., 2005, and others). The use of the hybrid method, in which the underlying components of the nonlinear shallow water equations (which form the basis of the Boussinesq model equations) are handled using the TVD finite volume method while dispersive terms are implemented using conventional finite differencing, provides a robust framework for modeling of surf zone flows. In particular, wave breaking may be handled entirely by the treatment of weak solutions in the shock-capturing TVD scheme, making the implementation of an explicit formulation for breaking wave dissipation unnecessary. In addition, shoreline movement may be handled quite naturally as part of the Reiman solver underlying the finite volume scheme.

In this version, we describe the development of a hybrid finite volume - finite difference scheme for the fully nonlinear Boussinesq model equations of Chen (2006), extended to incorporate a moving reference level as in Kennedy et al (2001). The use of a moving reference elevation is more consistent with a time-varying representation of elevation at a moving shoreline in modeling of a swash zone dynamics and coastal inundation. A conservative form of the equations is derived. Dispersive terms are reorganized with the aim of constructing a tridiagonal structure of spatial derivatives within time-derivative terms. The surface elevation gradient term are also rearranged to obtain a numerically well-balanced form, which is suitable for any numerical order. In contrast to previous high-order temporal schemes, which usually require uniform time-stepping, we use adaptive time stepping based on a third-order Runge-Kutta method. Spatial derivatives are discretized using a combination of finite-volume and finite-difference methods. A high-order MUSCL(Monotone Upstream-centered Schemes for Conservation Laws) reconstruction technique, which is accurate up to the fourth-order, is used in the Riemann solver. The wave breaking scheme follows the approach of Tonelli and Petti (2009), who used the ability of the nonlinear shallow water equations (NLSWE) with a TVD solver to simulate moving hydraulic jumps. Wave breaking is modeled by switching from Boussinesq to NSWE at cells where the Froude number exceeds a certain threshold. A wetting-drying scheme is used to model a moving shoreline.

The model was parallelized using the domain decomposition technique. The Message Passing Interface (MPI) with non-blocking communication is used for data communication between processors.

This report provides derivations of the conservation form of theoretical equations with a well-balanced pressure gradient term, numerical schemes, and users' manual. The last part of report illustrates the model's applications to problems of wave breaking and runup in the context of a standard suite of benchmark tests. In addition, we include a documentation of the spherical Boussinesq model used for Tsunami wave simulations. The spherical Boussinesq model was based on Kirby

et al. (2004, 2012) and implemented in the same model framework. A detailed documentation for the spherical code will be reported separately.

## 2 Theory

In this section, we describe the development of a set of Boussinesq equations which are accurate to  $O(\mu^2)$  in dispersive effects. Here,  $\mu$  is a parameter characterizing the ratio of water depth to wave length, and is assumed to be small in classical Boussinesq theory. We retain dimensional forms below but will refer to the apparent  $O(\mu^2)$  ordering of terms resulting from deviations from hydrostatic behavior in order to identify these effects as needed. The model equations used here follow from the work of Chen (2006). In this and earlier works starting with Nwogu (1993), the horizontal velocity is written as

$$\mathbf{u} = \mathbf{u}_\alpha + \mathbf{u}_2(z) \quad (1)$$

Here,  $\mathbf{u}_\alpha$  denotes the velocity at a reference elevation  $z = z_\alpha$ , and

$$\mathbf{u}_2(z) = (z_\alpha - z)\nabla A + \frac{1}{2}(z_\alpha^2 - z^2)\nabla B \quad (2)$$

represents the depth-dependent correction at  $O(\mu^2)$ , with  $A$  and  $B$  given by

$$\begin{aligned} A &= \nabla \cdot (h\mathbf{u}_\alpha) \\ B &= \nabla \cdot \mathbf{u}_\alpha \end{aligned} \quad (3)$$

The derivation follows Chen (2006) except for the additional effect of letting the reference elevation  $z_\alpha$  vary in time according to

$$z_\alpha = \zeta h + \beta \eta \quad (4)$$

where  $h$  is local still water depth,  $\eta$  is local surface displacement and  $\zeta$  and  $\beta$  are constants, as in Kennedy et al (2001). This addition does not alter the details of the derivation, which are omitted below.

### 2.1 Governing equations

The equations of Chen (2006) extended to incorporate a possible moving reference elevation follow. The depth-integrated volume conservation equation is given by

$$\eta_t + \nabla \cdot \mathbf{M} = 0 \quad (5)$$

where

$$\mathbf{M} = H \{ \mathbf{u}_\alpha + \bar{\mathbf{u}}_2 \} \quad (6)$$

is the horizontal volume flux.  $H = h + \eta$  is the total local water depth and  $\bar{\mathbf{u}}_2$  is the depth averaged  $O(\mu^2)$  contribution to the horizontal velocity field, given by

$$\bar{\mathbf{u}}_2 = \frac{1}{H} \int_{-h}^{\eta} \mathbf{u}_2(z) dz = \left( \frac{z_\alpha^2}{2} - \frac{1}{6}(h^2 - h\eta + \eta^2) \right) \nabla B + \left( z_\alpha + \frac{1}{2}(h - \eta) \right) \nabla A \quad (7)$$

The depth-averaged horizontal momentum equation can be written as

$$\mathbf{u}_{\alpha,t} + (\mathbf{u}_\alpha \cdot \nabla) \mathbf{u}_\alpha + g \nabla \eta + \mathbf{V}_1 + \mathbf{V}_2 + \mathbf{V}_3 + \mathbf{R} = 0 \quad (8)$$

where  $g$  is the gravitational acceleration and  $\mathbf{R}$  represents diffusive and dissipative terms including bottom friction and subgrid lateral turbulent mixing.  $\mathbf{V}_1$  and  $\mathbf{V}_2$  are terms representing the dispersive Boussinesq terms given by

$$\mathbf{V}_1 = \left\{ \frac{z_\alpha^2}{2} \nabla B + z_\alpha \nabla A \right\}_t - \nabla \left[ \frac{\eta^2}{2} B_t + \eta A_t \right] \quad (9)$$

$$\mathbf{V}_2 = \nabla \left\{ (z_\alpha - \eta)(\mathbf{u}_\alpha \cdot \nabla) A + \frac{1}{2}(z_\alpha^2 - \eta^2)(\mathbf{u}_\alpha \cdot \nabla) B + \frac{1}{2}[A + \eta B]^2 \right\} \quad (10)$$

The form of (9) allows for the reference level  $z_\alpha$  to be treated as a time-varying elevation, as suggested in Kennedy et al (2001). If this extension is neglected, the terms reduce to the form given originally by Wei et al (1995). The expression (10) for  $\mathbf{V}_2$  was also given by Wei et al (1995), and is not altered by the choice of a fixed or moving reference elevation.

The term  $\mathbf{V}_3$  in (8) represents the  $O(\mu^2)$  contribution to the expression for  $\boldsymbol{\omega} \times \mathbf{u} = \omega \mathbf{i}^z \times \mathbf{u}$  (with  $\mathbf{i}^z$  the unit vector in the  $z$  direction) and may be written as

$$\mathbf{V}_3 = \omega_0 \mathbf{i}^z \times \bar{\mathbf{u}}_2 + \omega_2 \mathbf{i}^z \times \mathbf{u}_\alpha \quad (11)$$

where

$$\omega_0 = (\nabla \times \mathbf{u}_\alpha) \cdot \mathbf{i}^z = v_{\alpha,x} - u_{\alpha,y} \quad (12)$$

$$\omega_2 = (\nabla \times \bar{\mathbf{u}}_2) \cdot \mathbf{i}^z = z_{\alpha,x}(A_y + z_\alpha B_y) - z_{\alpha,y}(A_x + z_\alpha B_x) \quad (13)$$

Following Nwogu (1993),  $z_\alpha$  is usually chosen in order to optimize the apparent dispersion relation of the linearized model relative to the full linear dispersion in some sense. In particular, the choice  $\alpha = (z_\alpha/h)^2/2 + z_\alpha/h = -2/5$  recovers a Padé approximant form of the dispersion relation, while the choice  $\alpha = -0.39$ , corresponding to the choice  $z_\alpha = -0.53h$ , minimizes the maximum error in wave phase speed occurring over the range  $0 \leq kh \leq \pi$ . Kennedy et al (2001) showed that, allowing  $z_\alpha$  to move up and down with the passage of the wave field, allowed a greater degree of flexibility in optimizing nonlinear behavior of the resulting model equations. In the examples chosen here, where a great deal of our focus is on the behavior of the model from the break point landward, we adopt Kennedy et al's "datum invariant" form

$$z_\alpha = -h + \beta H = (\beta - 1)h + \beta \eta = \zeta h + (1 + \zeta)\eta \quad (14)$$

with  $\zeta = -0.53$  as in Nwogu (1993) and  $\beta = 1 + \zeta = 0.47$ . This corresponds in essence to a  $\sigma$  coordinate approach, which places the reference elevation at a level 53% of the total local depth below the local water surface. This also serves to keep the model reference elevation within the actual water column over the entire wetted extent of the model domain.

## 2.2 Treatment of the surface gradient term

The hybrid numerical scheme requires a conservative form of continuity equation and momentum equations, thus requiring a modification of the leading order pressure term in the momentum equation. A numerical imbalance problem occurs when the surface gradient term is conventionally split into an artificial flux gradient and a source term that includes the effect of the bed slope for a non-uniform bed. To eliminate errors introduced by the traditional depth gradient method (DGM), a so-called surface gradient method (SGM) proposed by Zhou et al. (2001) was adopted in the TVD based-Boussinesq models in the recent literatures. Zhou et al. discussed an example of SGM in 1-D and verified that the slope-source term may be canceled out by part of the numerical flux term associated with water depth, if the bottom elevation at the cell center is constructed using the average of bottom elevations at two cell interfaces. Zhou et al. also showed a 2D application, but without explicitly describing 2D numerical schemes. Although this scheme can be extended into 2D following the same procedure as in 1D, it was found that the 2D extension may not be trivial in terms of the bottom construction for a 2D arbitrary bathymetry. Kim et al. (2008) pointed out that the water depth in the slope-source term should be written in a discretized form rather than the value obtained using the bottom construction, implying that their revised SGM is valid for general 2D applications.

For the higher-order schemes, such as the fourth-order MUSCL-TVD scheme (Yamamoto and Daiguji, 1993, Yamamoto et al., 1998) used in the recent Boussinesq applications, the original SGM and the revised SGM may not be effective in removing the artificial source. This problem was recently noticed by some authors, such as Roeber et al. (2010), who kept a first-order scheme (second-order for normal conditions) for the numerical flux term and the slope-source term in order to ensure a well-balanced solution, without adding noise for a rapidly varying bathymetry.

In fact, the imbalance problem can be solved by a reformulation of this term in terms of deviations from an unforced but separately specified equilibrium state (see general derivations in Rogers et al., 2003 and recent application in Liang and Marche, 2009). Using this technique, the surface gradient term may be split as

$$gH\nabla\eta = \nabla \left[ \frac{1}{2}g(\eta^2 + 2h\eta) \right] - g\eta\nabla h \quad (15)$$

which is well-balanced for any numerical order under an unforced stationary condition (still water condition).

### 2.3 Conservative form of fully nonlinear Boussinesq equations

For Chen's (2006) equations or the minor extension considered here,  $H\mathbf{u}_\alpha$  can be used as a conserved variable in the construction of a conservative form of Boussinesq equations, but this results in a source term in the mass conservation equation, such as in Shiach and Mingham (2009) and Roeber et al. (2010). An alternative approach is to use  $\mathbf{M}$  as a conserved variable in terms of the physical meaning of mass conservation. In this study, we used  $\mathbf{M}$ , instead of  $H\mathbf{u}_\alpha$ , in the following derivations of the conservative form of the fully nonlinear Boussinesq equations.

Using  $\mathbf{M}$  from (6) together with the vector identity

$$\nabla \cdot (\mathbf{u}\mathbf{v}) = \nabla\mathbf{u} \cdot \mathbf{v} + (\nabla \cdot \mathbf{v})\mathbf{u} \quad (16)$$

allows (8) to be rearranged as

$$\begin{aligned} & \mathbf{M}_t + \nabla \cdot \left( \frac{\mathbf{M}\mathbf{M}}{H} \right) + gH\nabla\eta \\ & = H \left\{ \bar{\mathbf{u}}_{2,t} + \mathbf{u}_\alpha \cdot \nabla\bar{\mathbf{u}}_2 + \bar{\mathbf{u}}_2 \cdot \nabla\mathbf{u}_\alpha - \mathbf{V}_1 - \mathbf{V}_2 - \mathbf{V}_3 - \mathbf{R} \right\} \end{aligned} \quad (17)$$

Following Wei et al. (1995), we separate the time derivative dispersion terms in  $\mathbf{V}_1$  according to

$$\mathbf{V}_1 = \mathbf{V}'_{1,t} + \mathbf{V}''_1 \quad (18)$$

where

$$\mathbf{V}'_1 = \frac{z_\alpha^2}{2} \nabla B + z_\alpha \nabla A - \nabla \left[ \frac{\eta^2}{2} B + \eta A \right] \quad (19)$$

and

$$\mathbf{V}''_1 = \nabla [\eta_t (A + \eta B)] \quad (20)$$

Using (15), (19) and (20), the momentum equation can be rewritten as

$$\begin{aligned} & \mathbf{M}_t + \nabla \cdot \left[ \frac{\mathbf{M}\mathbf{M}}{H} \right] + \nabla \left[ \frac{1}{2} g(\eta^2 + 2h\eta) \right] = \\ & = H \left\{ \bar{\mathbf{u}}_{2,t} + \mathbf{u}_\alpha \cdot \nabla\bar{\mathbf{u}}_2 + \bar{\mathbf{u}}_2 \cdot \nabla\mathbf{u}_\alpha - \mathbf{V}'_{1,t} - \mathbf{V}''_1 - \mathbf{V}_2 - \mathbf{V}_3 - \mathbf{R} \right\} + g\eta\nabla h \end{aligned} \quad (21)$$

A difficulty usually arises in applying the adaptive time-stepping scheme to the time derivative dispersive terms  $\bar{\mathbf{u}}_{2,t}$  and  $\mathbf{V}'_{1,t}$ , which was usually calculated using values stored in several time levels in the previous Boussinesq codes such as in Wei et al. (1995) and Shi et al. (2001). To prevent this, the equation can be re-arranged by merging the time derivatives on the right hand side into the time derivative term on the left hand side, giving

$$\begin{aligned} \mathbf{V}_t & + \nabla \cdot \left[ \frac{\mathbf{M}\mathbf{M}}{H} \right] + \nabla \left[ \frac{1}{2} g(\eta^2 + 2h\eta) \right] = \eta_t (\mathbf{V}'_1 - \bar{\mathbf{u}}_2) \\ & + H (\mathbf{u}_\alpha \cdot \bar{\mathbf{u}}_2 + \bar{\mathbf{u}}_2 \cdot \nabla\mathbf{u}_\alpha - \mathbf{V}''_1 - \mathbf{V}_2 - \mathbf{V}_3 - \mathbf{R}) + g\eta\nabla h \end{aligned} \quad (22)$$

where

$$\mathbf{V} = H(\mathbf{u}_\alpha + \mathbf{V}'_1) \quad (23)$$

In (23)  $\eta_t$  can be calculated explicitly using (5) as in Roeber et al. (2010). Equations (5) and (22) are the governing equations solved in this study. As  $\mathbf{V}$  is obtained, the velocity  $\mathbf{u}_\alpha$  can be found by solving a system of equation with tridiagonal matrix formed by (23), in which all cross-derivatives are moved to the right-hand side of the equation.

### 3 Numerical schemes

#### 3.1 Compact form of governing equations

We define

$$\begin{aligned} \mathbf{u}_\alpha &= (u, v), \\ \bar{\mathbf{u}}_2 &= (U_4, V_4), \\ \mathbf{M} &= (P, Q) = H [u + U_4, v + V_4], \\ \mathbf{V}'_1 &= (U'_1, V'_1), \\ \mathbf{V}''_1 &= (U''_1, V''_1), \\ \mathbf{V}_2 &= (U_2, V_2), \\ \mathbf{V} &= (U, V) = H [(u + U'_1), (v + V'_1)]. \end{aligned}$$

The generalized conservative form of Boussinesq equations can be written as

$$\frac{\partial \Psi}{\partial t} + \nabla \cdot \Theta(\Psi) = \mathbf{S} \quad (24)$$

where  $\Psi$  and  $\Theta(\Psi)$  are the vector of conserved variables and the flux vector function, respectively, and are given by

$$\Psi = \begin{pmatrix} \eta \\ U \\ V \end{pmatrix}, \quad \Theta = \begin{pmatrix} P\mathbf{i} + Q\mathbf{j} \\ \left[ \frac{P^2}{H} + \frac{1}{2}g(\eta^2 + 2\eta h) \right] \mathbf{i} + \frac{PQ}{H} \mathbf{j} \\ \frac{PQ}{H} \mathbf{i} + \left[ \frac{Q^2}{H} + \frac{1}{2}g(\eta^2 + 2\eta h) \right] \mathbf{j} \end{pmatrix}. \quad (25)$$

$$\mathbf{S} = \begin{pmatrix} 0 \\ g\eta \frac{\partial h}{\partial x} + \psi_x + HR_x \\ g\eta \frac{\partial h}{\partial y} + \psi_y + HR_y \end{pmatrix}, \quad (26)$$

where

$$\psi_x = \eta_t(U'_1 - U_4) + H (uU_{4,x} + vU_{4,y} + U_4u_x + V_4u_y - U''_1 - U_2 - U_3) \quad (27)$$

$$\psi_y = \eta_t(V_1' - V_4) + H(uV_{4,x} + vV_{4,y} + U_4v_x + V_4v_y - U_1'' - V_2 - V_3) \quad (28)$$

The expanded forms of  $(U_1', V_1')$ ,  $(U_1'', V_1'')$ ,  $(U_2, V_2)$ ,  $(U_3, V_3)$  and  $(U_4, V_4)$  can be found in Appendix A. For the term  $\mathbf{R}$ , the bottom stress is approximated using a quadratic friction equation. A Smagorinsky (1963)-like subgrid turbulent mixing algorithm is implemented following Chen et al. (1999).

### 3.2 Spatial discretization

A combined finite-volume and finite-difference method was applied to the spatial discretization. For the flux terms and the first-order derivative terms, a high-order MUSCL-TVD scheme is implemented in the present model. The high-order MUSCL-TVD scheme can be written in a compact form including different orders of accuracy from the second- to the fourth-order, according to Erduran et al. (2005) who modified Yamamoto et al.'s (1998) fourth-order approach. In  $x$ -direction, for example, the combined form of the interface construction can be written as follows:

$$\phi_{i+1/2}^L = \phi_i + \frac{1}{4} [(1 - \kappa_1)\chi(r)\Delta^*\phi_{i-1/2} + (1 + \kappa_1)\chi(1/r)\Delta^*\phi_{i+1/2}] \quad (29)$$

$$\phi_{i-1/2}^R = \phi_i - \frac{1}{4} [(1 + \kappa_1)\chi(r)\Delta^*\phi_{i-1/2} + (1 - \kappa_1)\chi(1/r)\Delta^*\phi_{i+1/2}] \quad (30)$$

where  $\phi_{i+1/2}^L$  is the constructed value at the left-hand side of the interface  $i + \frac{1}{2}$  and  $\phi_{i-1/2}^R$  is the value at the right-hand side of the interface  $i - \frac{1}{2}$ . The values of  $\Delta^*\phi$  are evaluated as follows:

$$\begin{aligned} \Delta^*\phi_{i+1/2} &= \Delta\phi_{i+1/2} - \kappa_2\Delta^3\bar{\phi}_{i+1/2}/6, \\ \Delta\phi_{i+1/2} &= \phi_{i+1} - \phi_i, \\ \Delta^3\bar{\phi}_{i+1/2} &= \Delta\bar{\phi}_{i+3/2} - 2\Delta\bar{\phi}_{i+1/2} + \Delta\bar{\phi}_{i-1/2}, \\ \Delta\bar{\phi}_{i-1/2} &= \text{minmod}(\Delta\phi_{i-1/2}, \Delta\phi_{i+1/2}, \Delta\phi_{i+3/2}), \\ \Delta\bar{\phi}_{i+1/2} &= \text{minmod}(\Delta\phi_{i+1/2}, \Delta\phi_{i+3/2}, \Delta\phi_{i-1/2}), \\ \Delta\bar{\phi}_{i+3/2} &= \text{minmod}(\Delta\phi_{i+3/2}, \Delta\phi_{i-1/2}, \Delta\phi_{i+1/2}) \end{aligned} \quad (31)$$

In (31), minmod represents the Minmod limiter and is given by

$$\text{minmod}(j, k, l) = \text{sign}(j)\max\{0, \min[|j|, 2\text{sign}(j)k, 2\text{sign}(j)l]\}. \quad (32)$$

$\kappa_1$  and  $\kappa_2$  in (29) and (30) are control parameters for orders of the scheme in the compact form. The complete form with  $(\kappa_1, \kappa_2) = (1/3, 1)$  is the fourth-order scheme given by Yamamoto et al. (1995).  $(\kappa_1, \kappa_2) = (1/3, 0)$  yields a third-order scheme, while the second-order scheme can be retrieved using  $(\kappa_1, \kappa_2) = (-1, 0)$ .

$\chi(r)$  in (29) and (30) is the limiter function. The original scheme introduced by Yamamoto et al. (1998) uses the Minmod limiter as used in (31). Erduran et al. (2005) found that the use of the van-Leer limiter for the third-order scheme gives more accurate results. Their finding was confirmed by using the present model in the benchmark tests for wave runoff conducted by Tehranirad et al. (2011). The van-Leer limiter can be expressed as

$$\chi(r) = \frac{r + |r|}{1 + r} \quad (33)$$

where

$$r = \frac{\Delta^* \phi_{i+1/2}}{\Delta^* \phi_{i-1/2}}. \quad (34)$$

The numerical fluxes are computed using a HLL approximate Riemann solver

$$\Theta(\Psi^L, \Psi^R) = \begin{cases} \Theta(\Psi^L) & \text{if } s_L \geq 0 \\ \Theta^*(\Psi^L, \Psi^R) & \text{if } s_L < 0 < s_R \\ \Theta(\Psi^R) & \text{if } s_R \leq 0, \end{cases} \quad (35)$$

where

$$\Theta^*(\Psi^L, \Psi^R) = \frac{s_R \Theta(\Psi^L) - s_L \Theta(\Psi^R) + s_L s_R (\Psi^R - \Psi^L)}{s_R - s_L} \quad (36)$$

The wave speeds of the Riemann solver are given by

$$s_L = \min(\mathbf{V}^L \cdot \mathbf{n} - \sqrt{g(h + \eta)^L}, u_s - \sqrt{\varphi_s}), \quad (37)$$

$$s_R = \max(\mathbf{V}^R \cdot \mathbf{n} + \sqrt{g(h + \eta)^R}, u_s + \sqrt{\varphi_s}), \quad (38)$$

in which  $u_s$  and  $\varphi_s$  are estimated as

$$u_s = \frac{1}{2}(\mathbf{V}^L + \mathbf{V}^R) \cdot \mathbf{n} + \sqrt{g(\eta + h)^L} - \sqrt{g(\eta + h)^R} \quad (39)$$

$$\sqrt{\varphi_s} = \frac{\sqrt{g(\eta + h)^L} + \sqrt{g(\eta + h)^R}}{2} + \frac{(\mathbf{V}^L - \mathbf{V}^R) \cdot \mathbf{n}}{4} \quad (40)$$

and  $\mathbf{n}$  is the normalized side vector for a cell face.

Higher derivative terms in  $\psi_x$  and  $\psi_y$  were discretized using a central difference scheme at the cell centroids, as in Wei et al. (1995). No discretization of dispersion terms at the cell interfaces is needed due to using  $\mathbf{M}$  as a flux variable. The Surface Gradient Method (Zhou et al, 2001) was used to eliminate unphysical oscillations. Because the pressure gradient term is re-organized as in section 2.2, there is no imbalance issue for the high-order MUSCL scheme.

### 3.3 Time stepping

The third-order Strong Stability-Preserving (SSP) Runge-Kutta scheme for nonlinear spatial discretization (Gottlieb et al., 2001) was adopted for time stepping. The scheme is given by

$$\begin{aligned}\Psi^{(1)} &= \Psi^n + \Delta t(-\nabla \cdot \Theta(\Psi^n) + \mathbf{S}^{(1)}) \\ \Psi^{(2)} &= \frac{3}{4}\Psi^n + \frac{1}{4}\left[\Psi^{(1)} + \Delta t\left(-\nabla \cdot \Theta(\Psi^{(1)}) + \mathbf{S}^{(2)}\right)\right] \\ \Psi^{n+1} &= \frac{1}{3}\Psi^n + \frac{2}{3}\left[\Psi^{(2)} + \Delta t\left(-\nabla \cdot \Theta(\Psi^{(2)}) + \mathbf{S}^{n+1}\right)\right]\end{aligned}\quad (41)$$

in which  $\Psi^n$  denotes  $\Psi$  at time level  $n$ .  $\Psi^{(1)}$  and  $\Psi^{(2)}$  are values at intermediate stages in the Runge-Kutta integration. As  $\Psi$  is obtained at each intermediate step, the velocity  $(u, v)$  can be solved by a system of tridiagonal matrix equations formed by (23).  $\mathbf{S}$  needs to be updated using  $(u, v, \eta)$  at the corresponding time step and an iteration is needed to achieve convergence.

An adaptive time step is chosen, following the Courant-Friedrichs-Lewy (CFL) criterion:

$$\Delta t = C \min \left( \min \frac{\Delta x}{|u_{i,j}| + \sqrt{g(h_{i,j} + \eta_{i,j})}}, \min \frac{\Delta y}{|v_{i,j}| + \sqrt{g(h_{i,j} + \eta_{i,j})}} \right) \quad (42)$$

where  $C$  is the Courant number and  $C = 0.5$  was used in the following examples.

### 3.4 Wave breaking and wetting-drying schemes for shallow water

The wave breaking scheme follows the approach of Tonelli and Petti (2009), who successfully used the ability of NSW E with a TVD scheme to model moving hydraulic jumps. Thus, the fully nonlinear Boussinesq equations are switched to NSW E at cells where the Froude number exceeds a certain threshold. Following Tonelli and Petti, the ratio of wave height to total water depth is chosen as the criterion to switch from Boussinesq to NSW E, with threshold value set to 0.8, as suggested by Tonelli and Petti.

The wetting-drying scheme for modeling a moving boundary is straightforward. The normal flux  $\mathbf{n} \cdot \mathbf{M}$  at the cell interface of a dry cell is set to zero. A mirror boundary condition is applied to the fourth-order MUSCL-TVD scheme and discretization of dispersive terms in  $\psi_x, \psi_y$  at dry cells. It may be noted that the wave speeds of the Riemann solver (37) and (38) for a dry cell are modified as

$$s_L = \mathbf{V}^L \cdot \mathbf{n} - \sqrt{g(h + \eta)^L}, \quad s_R = \mathbf{V}^L \cdot \mathbf{n} + 2\sqrt{g(h + \eta)^L} \quad (\text{right dry cell}) \quad (43)$$

and

$$s_L = \mathbf{V}^R \cdot \mathbf{n} - \sqrt{g(h + \eta)^R}, \quad s_R = \mathbf{V}^R \cdot \mathbf{n} + 2\sqrt{g(h + \eta)^R} \quad (\text{left dry cell}) \quad (44)$$

### 3.5 Boundary conditions, wavemaker and wind effect

We implemented various boundary conditions including wall boundary condition, absorbing boundary condition following Kirby et al. (1998) and periodic boundary condition following Chen et al. (2003).

Wavemakers implemented in this study include Wei and Kirby’s (1999) internal wavemakers for regular waves and irregular waves. For the irregular wavemaker, an extension was made to incorporate an alongshore periodicity into wave generation, in order to eliminate a boundary effect on wave simulations. The technique exactly follows the strategy in Chen et al. (2003), who adjusted the distribution of wave directions in each frequency bin to obtain alongshore periodicity. This approach is effective in modeling of breaking wave-induced nearshore circulation such as alongshore currents and rip currents.

Wind effects are modeled using the wind stress forcing proposed by Chen et al. (2004). The wind stress is expressed by

$$\mathbf{R}_w = \frac{\rho_a}{\rho} C_{dw} |\mathbf{U}_{10} - \mathbf{C}| (\mathbf{U}_{10} - \mathbf{C}) \quad (45)$$

where  $\rho_a$  and  $\rho$  represent air density and water density, respectively,  $\mathbf{C}$  is wave celerity. The wind stress is only applied on wave crests. A free parameter representing a ratio of the forced crest height to maximum surface elevation is implemented in the model.

### 3.6 Parallelization

In parallelizing the computational model, we used a domain decomposition technique to subdivide the problem into multiple regions and assign each subdomain to a separate processor core. Each subdomain region contains an overlapping area of ghost cells, three-row deep, as required by the fourth order MUSCL-TVD scheme. The Message Passing Interface (MPI) with non-blocking communication is used to exchange data in the overlapping region between neighboring processors. Velocity components are obtained from Equation (23), by solving tridiagonal matrices using the parallel pipelining tridiagonal solver described in Naik et al. (1993).

To investigate performance of the parallel program, numerical simulations of an idealized case are tested with different numbers of processors on a Linux cluster located at University of Delaware. The test case is set up in a numerical grid of  $1800 \times 1800$  cells. Figure 1 shows the model speedup versus number of processors. It can be seen that performance scales nearly proportional to the number of processors, with some delay caused by inefficiencies in parallelization, such as inter-processor communication time.

### 3.7 Implementation of weakly nonlinear Boussinesq equations in spherical coordinates

The weakly nonlinear Boussinesq equations in spherical coordinates are solved in the same model framework. We used the spherical Boussinesq equations derived by Kirby et al. (2004, 2012):

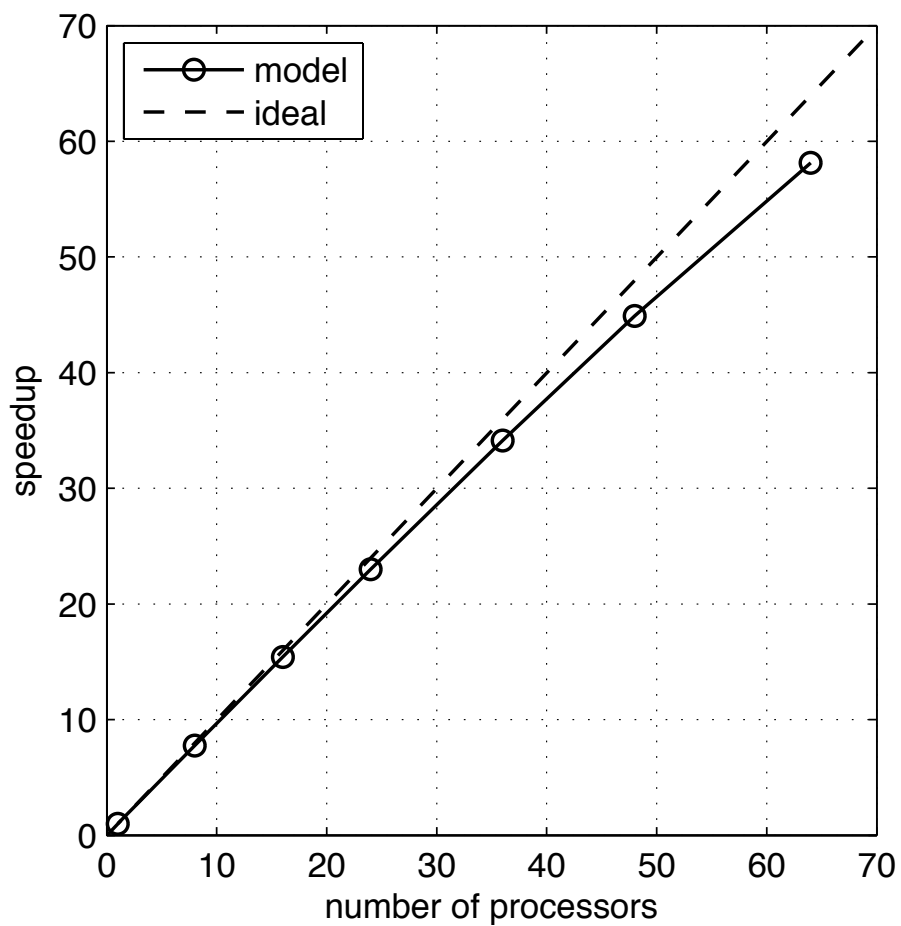


Figure 1: Variation in model performance with number of processors for a 1800 x 1800 domain. Straight line indicates arithmetic speedup. Actual performance is shown in the curved line.

$$H_t + \frac{1}{r_0 \cos \theta} \{ (Hu)_\phi + (Hv \cos \theta)_\theta \} = 0 \quad (46)$$

$$\begin{aligned} & u_t - fv + \frac{1}{r_0 \cos \theta} uu_\phi + \frac{1}{r_0} vu_\theta + \frac{g}{r_0 \cos \theta} \eta_\phi \\ & + \frac{1}{r_0^2 \cos^2 \theta} \left\{ \frac{h^2}{6} [u_{\phi\phi t} + (v \cos \theta)_{\phi\theta t}] - \frac{h}{2} [(hu_t)_{\phi\phi} + (h \cos \theta v_t)_{\phi\theta}] \right\} \\ & - \tau_b^\phi + \frac{1}{r_0 \cos \theta} (BFT)_\phi = 0 \end{aligned} \quad (47)$$

$$\begin{aligned} & v_t + fu + \frac{1}{r_0 \cos \theta} uv_\phi + \frac{1}{r_0} vv_\theta + \frac{g}{r_0} \eta_\theta \\ & + \frac{1}{r_0^2} \left\{ \frac{h^2}{6} \left[ \frac{1}{\cos \theta} \{u_{\phi t} + (v \cos \theta)_{\theta t}\} \right]_\theta - \frac{h}{2} \left[ \frac{1}{\cos \theta} \{ (hu_t)_\phi + (h \cos \theta v_t)_\theta \} \right]_\theta \right\} \\ & - \tau_b^\theta + \frac{1}{r_0} (BFT)_\theta = 0 \end{aligned} \quad (48)$$

where  $\theta$  and  $\phi$  denote latitude and longitude, respectively,  $r_0$  is the earth radius,  $f$  is the Coriolis parameter,  $H = h + \eta$ ,  $(u, v)$  represent the depth-averaged velocity.  $BFT$  denotes forcing terms resulting from motion of the ocean bottom and it is not taken into account in the present program.

To facilitate solving the spherical equations in the same model framework as in the Cartesian coordinates, we solve the spherical governing equations by transforming the equations into an equivalent set of equations in Cartesian coordinates using a standard cylindrical projection. We define

$$\begin{cases} \xi_1 = r_0 \cos \theta_0 (\phi - \phi_0) \\ \xi_2 = r_0 (\theta - \theta_0) \end{cases} \quad (49)$$

where  $(\phi_0, \theta_0)$  are the reference longitude and latitude, respectively. The differentials of  $\xi_1$  and  $\xi_2$  are

$$\begin{cases} d\xi_1 = r_0 \cos \theta_0 d\phi \\ d\xi_2 = r_0 d\theta \end{cases} \quad (50)$$

$d\phi$  and  $d\theta$  in (46) - (48) are replaced by  $d\xi_1$  and  $d\xi_2$ . Detailed derivations for each term are described below.

$$\frac{1}{r_0 \cos \theta} (Hu)_\phi = S_p (Hu)_{\xi_1} \quad (51)$$

$$\frac{1}{r_0 \cos \theta} (Hv \cos \theta)_\theta = \frac{1}{r_0 \cos \theta} [\cos \theta (Hv)_\theta - Hv \sin \theta] = (Hv)_{\xi_2} - \frac{1}{r_0} \tan \theta Hv \quad (52)$$

$$\frac{1}{r_0 \cos \theta} uu_\phi = S_p uu_{\xi_1} \quad (53)$$

$$\frac{1}{r_0} vv_\theta = vv_{\xi_2} \quad (54)$$

$$\frac{1}{r_0 \cos \theta} g\eta_\phi = S_p g\eta_{\xi_1} \quad (55)$$

$$\frac{h^2}{6} \frac{1}{r_0^2 \cos^2 \theta} u_{\phi\phi t} = S_p^2 \frac{h^2}{6} u_{\xi_1 \xi_1 t} \quad (56)$$

$$\frac{h^2}{6} \frac{1}{r_0^2 \cos^2 \theta} (v \cos \theta)_{\phi\theta t} = \frac{h^2 S_p}{6} \left( v_{\xi_1 \xi_2} - \frac{1}{r_0} \tan \theta v_{\xi_1} \right)_t \quad (57)$$

$$-\frac{h}{2} \frac{1}{r_0^2 \cos^2 \theta} (hu)_{\phi\phi t} = -\frac{h S_p^2}{2} (hu)_{\xi_1 \xi_1 t} \quad (58)$$

$$-\frac{h}{2} \frac{1}{r_0^2 \cos^2 \theta} (hv \cos \theta)_{\phi\theta t} = -\frac{h S_p}{2} \left[ (hv)_{\xi_1 \xi_2} - \frac{1}{r_0} \tan \theta (hv)_{\xi_1} \right]_t \quad (59)$$

$$\frac{1}{r_0 \cos \theta} uv_\phi = S_p uv_{\xi_1} \quad (60)$$

$$\frac{1}{r_0} vv_\theta = vv_{\xi_2} \quad (61)$$

$$\frac{1}{r_0} g\eta_\theta = g\eta_{\xi_2} \quad (62)$$

$$\frac{h^2}{6} \frac{1}{r_0^2} \left( \frac{u_{\phi t}}{\cos \theta} \right)_\theta = \frac{h^2 S_p}{6} \left( u_{\xi_1 \xi_2} + \frac{1}{r_0} \tan \theta u_{\xi_1} \right)_t \quad (63)$$

$$-\frac{h}{2} \frac{1}{r_0^2} \left[ \frac{(hu)_{\phi t}}{\cos \theta} \right]_\theta = -\frac{h S_p}{2} \left[ (hu)_{\xi_1 \xi_2} + \frac{1}{r_0} \tan \theta (hu)_{\xi_1} \right]_t \quad (64)$$

$$\frac{h^2}{6} \frac{1}{r_0^2} \left[ \frac{(v \cos \theta)_{\theta t}}{\cos \theta} \right]_\theta = \frac{h^2}{6} \left[ v_{\xi_2 \xi_2} - \frac{1}{r_0} \tan \theta v_{\xi_2} - \frac{1}{r_0^2 \cos^2 \theta} v \right]_t \quad (65)$$

$$-\frac{h}{2} \frac{1}{r_0^2} \left[ \frac{(hv \cos \theta)_{\theta t}}{\cos \theta} \right]_\theta = -\frac{h}{2} \left[ (hv)_{\xi_2 \xi_2} - \frac{1}{r_0} \tan \theta (hv)_{\xi_2} - \frac{1}{r_0^2 \cos^2 \theta} hv \right]_t \quad (66)$$

where  $S_p$  is a spherical coordinate correction factor expressed by

$$S_p = \frac{\cos \theta_0}{\cos \theta}. \quad (67)$$

The equations in  $(\xi_1, \xi_2)$  coordinates are

$$H_t + S_p (Hu)_{\xi_1} + (Hv)_{\xi_2} = \frac{1}{r_0} \tan \theta H v \quad (68)$$

$$u_t + S_p uu_{\xi_1} + vv_{\xi_2} - f v + S_p g\eta_{\xi_1} + F_t - \tau_b^{\xi_1} + S_p (BFT)_{\xi_1} = 0 \quad (69)$$

$$v_t + S_p uv_{\xi_1} + vv_{\xi_2} + fu + g\eta_{\xi_2} + G_t - \tau_b^{\xi_2} + (BFT)_{\xi_2} \quad (70)$$

where

$$F = \frac{h^2 S_p^2}{6} u_{\xi_1 \xi_1} + \frac{h^2 S_p}{6} (v_{\xi_1 \xi_2} - \frac{1}{r_0} \tan \theta v_{\xi_1}) - \frac{h S_p^2}{2} (hu)_{\xi_1 \xi_1} - \frac{h S_p}{2} \left[ (hv)_{\xi_1 \xi_2} - \frac{1}{r_0} \tan \theta (hv)_{\xi_1} \right] \quad (71)$$

$$G = \frac{h^2 S_p}{6} \left( u_{\xi_1 \xi_2} + \frac{1}{r_0} \tan \theta u_{\xi_1} \right) + \frac{h^2}{6} \left( v_{\xi_2 \xi_2} - \frac{1}{r_0} \tan \theta v_{\xi_2} - \frac{1}{r_0^2 \cos^2 \theta} v \right) - \frac{h S_p}{2} \left[ (hu)_{\xi_1 \xi_2} + \frac{1}{r_0} \tan \theta (hu)_{\xi_1} \right] - \frac{h}{2} \left[ (hv)_{\xi_2 \xi_2} - \frac{1}{r_0} \tan \theta (hv)_{\xi_2} - \frac{1}{r_0^2 \cos^2 \theta} (hv) \right] \quad (72)$$

The conservation forms of the spherical equations can be rewritten in the same form of the Cartesian equations (24) and  $\Psi$ ,  $\Theta$  and  $\mathbf{S}$  are defined as

$$\Psi = \begin{pmatrix} \eta \\ U_s \\ V_s \end{pmatrix}, \quad \Theta = \begin{pmatrix} S_p P \mathbf{i} + Q \mathbf{j} \\ \left[ \frac{S_p P^2}{h+\eta} + \frac{1}{2} S_p g (\eta^2 + 2\eta h) \right] \mathbf{i} + \frac{PQ}{h+\eta} \mathbf{j} \\ \frac{S_p P Q}{h+\eta} \mathbf{i} + \left[ \frac{Q^2}{h+\eta} + \frac{1}{2} g (\eta^2 + 2\eta h) \right] \mathbf{j} \end{pmatrix}. \quad (73)$$

$$\mathbf{S} = \begin{pmatrix} \frac{1}{r_0} \tan \theta (h + \eta) v \\ S_p g \eta \frac{\partial h}{\partial \xi_1} + f(h + \eta) v + \tau_b^{\xi_1} + \psi_1 \\ g \eta \frac{\partial h}{\partial \xi_2} - f(h + \eta) u + \tau_b^{\xi_2} + \psi_2 \end{pmatrix}, \quad (74)$$

where  $P = (h + \eta)u$ ,  $Q = (h + \eta)v$ ,

$$U_s = (h + \eta)(u + F) \quad (75)$$

$$V_s = (h + \eta)(v + G) \quad (76)$$

$$\psi_1 = \eta_t F \quad (77)$$

$$\psi_2 = \eta_t G \quad (78)$$

## 4 Users' Manual

### 4.1 Program outline and flow chart

The code was written using Fortran 90 with the `c` preprocessor (`cpp`) statements for separation of the source code. Arrays are dynamically allocated at runtime. Precision is selected using the `selected_real_kind` Fortran intrinsic function defined in the makefile. The default precision is single.

The present version of FUNWAVE-TVD includes a number of options including (1) choice of serial or parallel code (2) Cartesian or spherical coordinate (Tsunami propagation mode), (3) samples, (4) one-way nesting mode, and (5) wave breaking index and aging (bubble and foam mode).

The flow chart is shown in Figure 2.

### 4.2 Subroutine and function descriptions

**ALLOCATE\_VARIABLES:** allocate variables. It is called by MAIN.

**BREAKING:** print breaking index and breaking age calculated based on Kennedy et al. (2000). This option is defined in `input.txt`.

**BOUNDARY\_CONDITION:** provide boundary conditions at four side boundaries. It is called by FLUXES.

**CAL\_DISPERSION:** calculate dispersion terms. The first and second derivatives with respect to  $x, y$  are also calculated in this subroutine. In addition, the dispersion values in ghost cells are updated in this subroutine. It is called by the main program.

**CALCULATE\_Cm\_Sm:** calculate  $C_m$  and  $S_m$  used in Wei and Kirby's internal wave maker for irregular waves (TMA). Detailed formulation can be found in Shi et al. (2003). The subroutine is called by INITIALIZATION.

**CALCULATE\_MEAN:** calculate mean  $u, v$  required by the smagorinsky mixing. Mean  $\eta$  is also calculated. Called by MAIN.

**CALCULATE\_SPONGE:** setup sponge layer. It is called by INITIALIZATION.

**CONSTRUCTION:** second- and third-order interface construction. It is called by FLUXES. It calls `CONSTRUCT_X` and `CONSTRUCT_Y`.

**CONSTRUCTION\_HO:** high order interface construction. It is called by FLUXES. It calls `CONSTRUCT_HO_X` and `CONSTRUCT_HO_Y`.

**CONSTRUCT\_HO\_X:** high order interface construction of specific variables in  $x$  direction. It is called by `CONSTRUCTION_HO`.

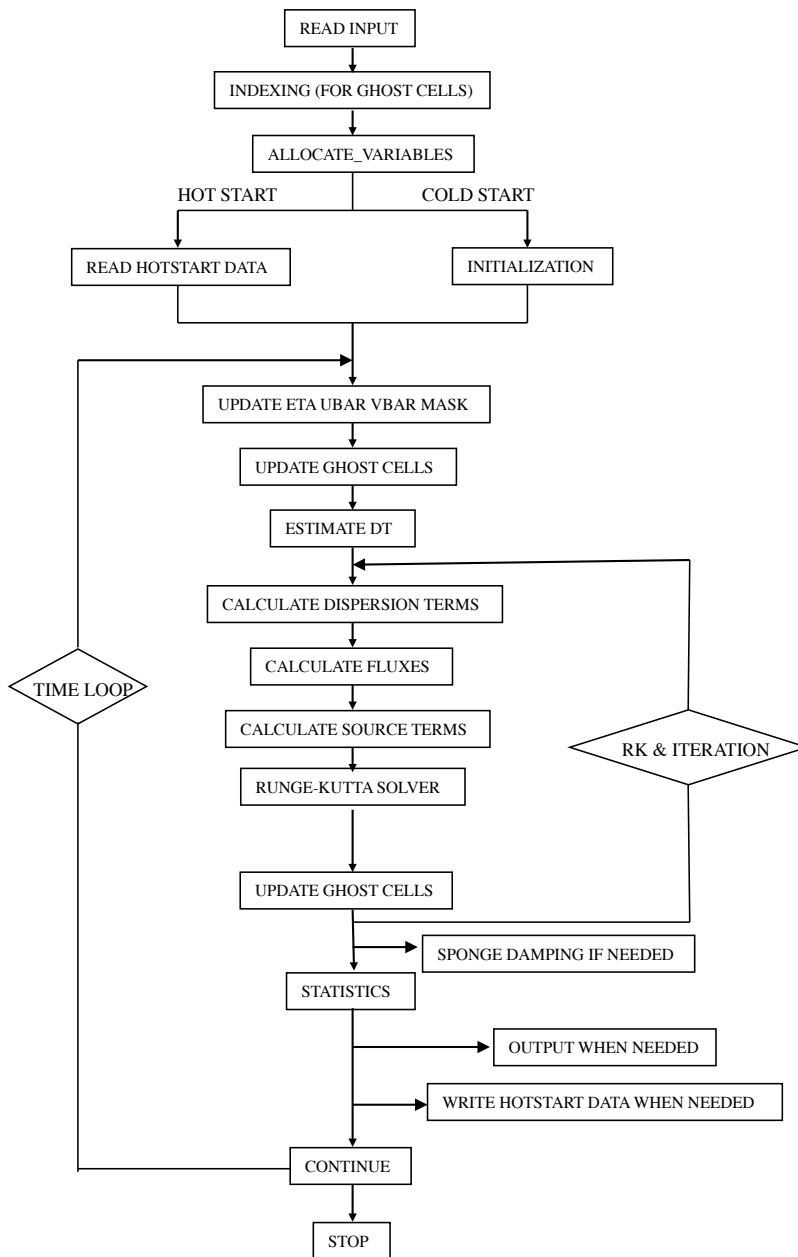


Figure 2: Flow chart of the main program.

**CONSTRUCT\_HO\_Y:** high order interface construction of specific variables in  $y$  direction. It is called by CONSTRUCTION\_HO.

**CONSTRUCT\_X:** construct variables in  $x$  direction. It is called by CONSTRUCTION.

**CONSTRUCT\_Y:** construct variables in  $y$  direction. It is called by CONSTRUCTION.

**CORRECTOR:** corrector time scheme. It was used for a comparison between Predictor-corrector scheme and Runge-Kutta. It is not suggested using it in the present program.

**DelxFun:** calculate derivatives with respect to  $x$ . It is called by DelxFun.

**DelxyFun:** calculate derivatives with respect to  $x$  and  $y$ . It is called by FLUXES when the lower order construction is applied. It calls DelxFun and DelyFun.

**DelyFun:** calculate derivatives with respect to  $y$ . It is called by DelxyFun.

**DERIVATIVE\_X:** calculate first-derivative respect to  $x$  in second order. The subroutine is called by CAL\_DISPERSION.

**DERIVATIVE\_X\_High:** calculate first-derivative respect to  $x$  in higher-order. The subroutine is called by CAL\_DISPERSION.

**DERIVATIVE\_XX:** calculate second-derivative respect to  $x$ . The subroutine is called by CAL\_DISPERSION.

**DERIVATIVE\_XY:** calculate cross-derivative. The subroutine is called by CAL\_DISPERSION.

**DERIVATIVE\_Y:** calculate first-derivative respect to  $y$  in second order. The subroutine is called by CAL\_DISPERSION.

**DERIVATIVE\_Y\_High:** calculate first-derivative respect to  $y$  in higher-order. The subroutine is called by CAL\_DISPERSION.

**DERIVATIVE\_YY:** calculate second-derivative respect to  $y$ . The subroutine is called by CAL\_DISPERSION.

**ESTIMATE\_DT:** evaluate dt based on CFL criteria. It is called by MAIN.

**ESTIMATE\_HUV:** Runge-Kutta solver. It is called by MAIN. It calls GET\_Eta\_U\_V\_HU\_HV.

**EXCHANGE:** update  $\eta, u, v, Hu, Hv$  and MASK in the ghost cells. It is called by MAIN. It calls PHI\_COLL.

**EXCHANGE\_DISPERSION:** update dispersion variables in the ghost cells. It is called by MAIN. It calls PHI\_COLL.

**FLUX\_AT\_INTERFACE:** calculate numerical fluxes at four cell interfaces using the averaging method. It is called by FLUXES.

**FLUX\_AT\_INTERFACE\_HLLC:** calculate numerical fluxes at four cell interfaces using HLLC scheme. It is called by FLUXES. It calls HLLC.

**FLUXES:** calculate numerical fluxes. It is called by MAIN. It calls CONSTRUCTION lower order or CONSTRUCTION\_HO for higher order, WAVE\_SPEED, DelxyFun (for lower order), FLUX\_AT\_INTERFACE\_HLLC for HLL scheme or FLUX\_AT\_INTERFACE for averaging scheme, and BOUNDARY\_CONDITION.

**GET\_Eta\_U\_V\_HU\_HV:** calculate  $\eta, u, v, Hu$  and  $Hv$ . It is called by ESTIMATE\_HUV. The tridiagonal solver is used to get  $u$  and  $v$ . Froude number cap is applied in this subroutine. It calls TRIG (wall boundary) or TRIG\_PERIODIC (periodic boundary). In the parallel mode, it calls TRIDx and TRIDy.

**GetFile:** read data in the global dimension and distribute to all processors in the parallel mode. Use flag '-DPARALLEL' in Makefile to include this subroutine.

**GatherVariable:** gather variables from all processors to processor 0 in the parallel mode but with serial tridiagonal solver. Use flag '-DTRID\_NO\_PARALLEL' to include this subroutine. It is called by TRIDxyNoParallel.

**HLLC:** HLLC scheme. It is called by FLUX\_AT\_INTERFACE\_HLLC.

**INDEX:** indexing for ghost cells and MPI subdomains. It is called by MAIN.

**INITIALIZATION:** initialization subroutine. It is called MAIN. It may call WK\_WAVEMAKER\_REGULAR\_WAVE, WK\_WAVEMAKER\_IRREGULAR\_WAVE, CALCULATE\_Cm\_Sm, CALCULATE\_SPONGE if applied.

**INITIAL\_GAUSSIAN:** sample to provide initial Gaussian hump. Use flag '-DSAMPLE' in Makefile to include this subroutine. Parameters are defined in input.txt. The subroutine is called by INITIALIZATION.

**INITIAL\_HOTSTART:** initialization when hotstart option is applied. It is called by MAIN. It may call INITIAL\_UVZ, INITIAL\_SOLITARY\_WAVE, INITIAL\_N\_WAVE, INITIAL\_RECTANGULAR, INITIAL\_WAVE, WK\_WAVEMAKER\_REGULAR\_WAVE, WK\_WAVEMAKER\_IRREGULAR\_WAVE, CALCULATE\_Cm\_Sm, CALCULATE\_SPONGE if applied.

**INITIAL\_N\_WAVE:** sample to provide initial N wave solution. Use flag '-DSAMPLE' in Makefile to include this subroutine. Parameters are defined in input.txt. The subroutine is called by INITIALIZATION.

**INITIAL\_SOLITARY\_WAVE:** sample to provide initial solitary wave solution. Use flag '-DSAMPLE' in Makefile to include this subroutine. Parameters are defined in input.txt. The subroutine is called by INITIALIZATION. It calls SUB\_SLTRY to get parameters.

**INITIAL\_RECTANGULAR:** sample of given an initial rectangular hump. Use flag ‘-DSAMPLE’ in Makefile to include this subroutine. Parameters are defined in input.txt. The subroutine is called by INITIALIZATION.

**INITIAL\_UVZ:** read initial  $u, v$ , and  $\eta$  data from files defined in input.txt. It is called by INITIALIZATION. It calls GetFile.

**MINMOD\_LIMITER:** function of minmod limiter. It is used in CONSTRUCT\_HO\_X, and CONSTRUCT\_HO\_Y.

**MPI\_INITIAL:** initialize MPI environment.

**OneWayCoupling:** one-way nesting subroutine. The nesting data read from INITIALIZATION.

**PHI\_EXCH:** handle float type data exchange between processors in the parallel mode. It is called by PHI\_COLL. Use flag ‘-DPARALLEL’ to include this subroutine.

**PHI\_INT\_EXCH:** handle integer type data exchange between processors in the parallel mode. It is called by UPDATE\_MASK. Use flag ‘-DPARALLEL’ to include this subroutine.

**PREDICTOR:** predictor scheme. It was used for a comparison between Predictor-corrector scheme and Runge-Kutta. It is not suggested using it in the present program.

**PREVIEW:** output subroutine. It is called by MAIN. It calls PutFile.

**PutFile:** print out output in files. In the parallel mode, it gathers data from all processors into processor 0 and prints out in the global dimension. Use flag ‘-DPARALLEL’ in Makefile for the parallel mode. It is called by PREVIEW.

**PHI\_COLL:** update data in ghost cells. It is called by EXCHANGE. in the parallel mode, it calls PHI\_EXCH which is a major subroutine to handle data exchange between processors.

**READ\_INPUT:** read input.txt. It is called by MAIN. It calls GET\_STRING\_VAL, GET\_LOGICAL\_VAL, GET\_INTEGER\_VAL, GET\_Float\_VAL. Input data are written out in LOG.txt.

**READ\_HOTSTART\_DATA:** read saved data for hot start and initialize other variables.

**ScatterVariable:** scatter variables from processor 0 to all processors in the parallel mode but with serial tridiagonal solver. Use flag ‘-DTRID\_NO\_PARALLEL’ to include this subroutine. It is called by TRIDxyNoParallel.

**SOLITARY\_WAVE\_LEFT\_BOUNDARY:** nudging boundary condition of solitary wave at left boundary. Use flag ‘-DSAMPLE’ in Makefile to include this subroutine. Parameters are defined in input.txt.

**SourceTerms:** calculate all source terms including slope term and dispersion terms. It is called by MAIN.

**STATISTICS:** calculate statistics of total mass volume, energy, maximum and minimum  $\eta, u, v$ , Froude number etc.

**SPONGE\_DAMPING:** use sponge layers to damp waves Parameters are defined in input.txt.

**SUB\_SLTRY:** provide solitary wave solution of Nogu's equations. It is called by INITIAL\_SOLITARY\_WAVE. Use flag '-DSAMPLE' in Makefile to include this subroutine.

**TRIGE:** tridiagonal solver. It allows diagonal variables not equal to unit. It is called by TRIG\_PERIODIC.

**TRIG:** tridiagonal solver. It is called by GET\_Eta\_U\_V\_HU\_HV. It calls TRIGE.

**TRIDxyNoParallel:** no parallel tridiagonal solver but in the parallel mode. It is only for testing. Use flag '-DTRID\_NO\_PARALLEL' to include this subroutine. It calls GatherVariable, TRIG and ScatterVariable.

**TRIG\_PERIODIC:** cyclic tridiagonal solver. It is called by GET\_Eta\_U\_V\_HU\_HV. It calls TRIGE.

**UPDATE\_MASK:** update mask according to wetting and drying. Also update mask and mask9 in ghost cells.

**VANLEER\_LIMITER:** function of Vanleer limiter. It is used in DelxFun and DelyFun.

**WAVE\_SPEED:** calculate numerical wave speed needed by the TVD scheme. It is called by MAIN.

**WK\_WAVEMAKER\_IRREGULAR\_WAVE:** calculate source function for Wei and Kirby's internal wave maker for irregular waves (TMA). Periodic boundary conditions are included. Parameters are defined in input.txt. The subroutine is called by INITIALIZATION.

**WK\_WAVEMAKER\_REGULAR\_WAVE:** calculate source function for Wei and Kirby's internal wave maker for regular waves. Periodic boundary conditions are included but for certain wave angles (will ask during a run). Parameters are defined in input.txt. The subroutine is called by INITIALIZATION.

**WRITE\_HOTSTART\_DATA:** write out data used for hot start.

### 4.3 Permanent variables

Depth(): still water depth  $h$  at element point

DepthNode(): still water depth  $h$  at node

DepthX(): still water depth  $h$  at x-interface

DepthY(): still water depth  $h$  at y-interface

Eta(): surface elevation, for dry point,  $\text{Eta}() = \text{MinDepth} - \text{Depth}()$ , MinDepth is specified in input.txt.

Eta0():  $\eta$  at previous time level

MASK(): 1 - wet, 0 - dry

MASK\_STRUC(): 0 - permanent dry point

MASK9: mask to switch from Boussinesq equation to SWE, 1 - Boussinesq, 0 - SWE

U(): depth-averaged  $u$  or  $u$  at the reference level ( $u_\alpha$ ) at element

V(): depth-averaged  $v$  or  $v$  at the reference level ( $v_\alpha$ ) at element

HU():  $(h + \eta)u$  at element

HV():  $(h + \eta)v$  at element

P():  $(h + \eta)(u + U_4)$  at x-interface

Q():  $(h + \eta)(v + V_4)$  at y-interface

Fx(): numerical flux F at x-interface

Fy(): numerical flux F at y-interface

Gx(): numerical flux G at x-interface

Gy(): numerical flux G at y-interface

Ubar():  $U$

Vbar():  $V$

U4(): x-component of  $U_4$

V4(): y-component of  $V_4$

U1p(): x-component of  $U'_1$

V1p(): y-component of  $V'_1$

EtaRxL():  $\eta$  Left value at x-interface

EtaRxR():  $\eta$  Right value at x-interface

EtaRyL():  $\eta$  Left value at y-interface

EtaRyR():  $\eta$  Right value at y-interface

HxL(): total depth Left value at x-interface

HxR(): total depth Right value at x-interface

HyL(): total depth Left value at y-interface

HyR(): total depth Right value at y-interface

HUxL():  $(h + \eta)u$  Left value at x-interface

HUxR():  $(h + \eta)u$  Right value at x-interface

HVyL():  $(h + \eta)v$  Left value at y-interface

HVyR():  $(h + \eta)v$  Right value at y-interface

PL():  $(h + \eta)(u + U_4)$ , Left value at x-interface

PR():  $(h + \eta)(u + U_4)$ , Right value at x-interface

QL():  $(h + \eta)(v + V_4)$ , Left value at y-interface

QR():  $(h + \eta)(v + V_4)$ , Right value at y-interface

FxL = HUxL\*UxL + 1/2\*g\*(EtaRxL<sup>2</sup> + 2\*EtaRxL\*Depthx)

FxR = HUxR\*UxR + 1/2\*g\*(EtaRxR<sup>2</sup> + 2\*EtaRxR\*Depthx)

FyL = HyL\*UyL\*VyL

FyR = HyR\*UyR\*VyR

GxL = HxL\*UxL\*VxL

GxR = HxR\*UxR\*VxR

GyL = HVyL\*VyL + 1/2\*g\*(EtaRyL<sup>2</sup> + 2\*EtaRyL\*Depthy)

GyR = HVyR\*VyR + 1/2\*g\*(EtaRyR<sup>2</sup> + 2\*EtaRyR\*Depthy)

## 4.4 Installation and compilation

FUNWAVE-TVD is distributed in a compressed file. To install the programs, first, uncompress the package. Then use

```
> tar xvf *.tar
```

to extract files from the uncompressed package. The extracted files will be distributed in two new directories: /src and /work.

To compile the program, go to /src and modify Makefile if needed. There are several necessary flags in Makefile needed to specify below.

- DDOUBLE\_PRECISION: use double precision, default is single precision.
  - DPARALLEL: use parallel mode, default is serial mode.
  - DSAMPLES: include all samples, default is no sample included.
  - DCARTESIAN: Cartesian version, otherwise Spherical version
  - DINTEL: if INTEL compiler is used, this option can make use of FPORT for the RAND() function
  - DMIXING: include Smagorinsky mixing.
  - DCOUPPING: nesting mode.
  - DMANNING: Using Manning coefficient for friction calculation.
- CPP: path to CPP directory.
- FC: Fortran compiler.

Then execute

```
> make
```

The executable file 'mytvd' will be generated and copied from /src to /work/. Note: use 'make clean' after modifying Makefile.

To run the model, go to /work. Modify input.txt if needed and run.

## 4.5 Input

Following are descriptions of parameters in input.txt (**NOTE:** all parameter names are capital sensitive).

**TITLE:** title of your case, only used for log file.

**SPECIFICATION OF HOT START**

HOT\_START: logical parameter, T for hot start, F for cold start.

FileNumber\_HOTSTART: number of hotstart file used for a hot start, e.g., 1,2, ...

### **SPECIFICATION OF MULTI-PROCESSORS**

PX: processor numbers in X

PY : processor numbers in Y

**NOTE:** PX and PY must be consistency with number of processors defined in mpirun command, e.g., mpirun -np n (where  $n = px \times py$ )

### **SPECIFICATION OF WATER DEPTH**

DEPTH\_TYPE: depth input type.

DEPTH\_TYPE=DATA: from a depth file.

The program includes several simple bathymetry configurations such as

DEPTH\_TYPE=FLAT: flat bottom, need DEPTH\_FLAT

DEPTH\_TYPE=SLOPE: plane beach along  $x$  direction. It needs three parameters: slope, SLP, slope starting point, Xslp and flat part of depth, DEPTH\_FLAT

DEPTH\_FILE: bathymetry file if DEPTH\_TYPE=DATA

DEPTH\_FLAT: water depth of flat bottom if DEPTH\_TYPE=FLAT or DEPTH\_TYPE=SLOPE (flat part of a plane beach).

SLP: slope if DEPTH\_TYPE=SLOPE

Xslp: starting  $x$  (m) of a slope, if DEPTH\_TYPE=SLOPE

### **SPECIFICATION OF RESULT FOLDER**

RESULT\_FOLDER: result folder name, e.g., RESULT\_FOLDER = /Users/fengyanshi/tmp/

### **SPECIFICATION OF DIMENSION**

Mglob: global dimension in  $x$  direction.

Nglob: global dimension in  $y$  direction.

### **SPECIFICATION OF TIME**

TOTAL\_TIME: simulation time in seconds

PLOT\_INTV: output interval in seconds (Note, output time is not exact because adaptive dt is used.)

SCREEN\_INTV: time interval (s) of screen print.

PLOT\_INTV\_STATION: time interval (s) of gauge output

HOTSTART\_INTV: time interval (s) to save hot start data.

### **SPECIFICATION OF GRID SIZE**

DX: grid size(m) in  $x$  direction.

DY: grid size(m) in  $y$  direction.

### **SPECIFICATION OF INITIAL CONDITION**

INT\_UVZ : logical parameter for initial condition, default is FALSE

ETA\_FILE: name of file for initial  $\eta$ , e.g., ETA\_FILE= /Users/fengyanshi/work/input/CVV\_H.grd, data format is the same as depth data.

U\_FILE: name of file for initial  $u$ , e.g., U\_FILE= /Users/fengyanshi/work/input/CVV\_U.grd, data format is the same as depth data.

V\_FILE: name of file for initial  $v$ , e.g., V\_FILE= /Users/fengyanshi/work/input/CVV\_V.grd, data format is the same as depth data.

### **SPECIFICATION OF WIND EFFECT**

WindForce: logical parameter representing if wind effect is taken into account. T or F. Note: spatially uniform wind field is assumed in this version.

WIND\_FILE: file name for wind data. The following is an example of data format.

```
wind data
100 - number of data
0.0 , 10.0 0.0 — time(s), wu, wv (m/s)
2000.0, 10.0, 0.0
8000.0, 10.0, 0.0
...
```

Cdw: wind stress coefficient for the quadratic formula.

WindCrestPercent: ratio of the forced wave crest height to the maximum surface elevation.

### **SPECIFICATION OF WAVEMAKER**

WAVEMAKER: wavemaker type.

WAVEMAKER = INI\_REC: initial rectangular hump, need Xc,Yc and WID

WAVEMAKER = LEF\_SOL: left boundary solitary, need AMP,DEP, and LAGTIME

WAVEMAKER = INI\_SOL: initial solitary wave, WKN B solution, need AMP, DEP, and XWAVEMAKER

WAVEMAKER = INI\_OTH: other initial distribution specified by users

WAVEMAKER = WK\_REG: Wei and Kirby 1999 internal wave maker, need Xc\_WK, Tperiod, AMP\_WK, DEP\_WK, Theta\_WK, and Time\_ramp (factor of period)

WAVEMAKER = WK\_IRR: Wei and Kirby 1999 TMA spectrum wavemaker, need Xc\_WK, DEP\_WK, Time\_ramp, Delta\_WK, FreqPeak, FreqMin,FreqMax, Hmo, GammaTMA, Theta-Peak

WAVEMAKER = WK\_TIME\_SERIES: *fft* a time series to get each wave component and then use Wei and Kirby's (1999) wavemaker. Need input WaveCompFile (including 3 columns: per,amp,pha) and NumWaveComp,PeakPeriod,DEP\_WK, Xc\_WK,Ywidth\_WK

WAVEMAKER = GAUSSIAN: initial Gaussian hump, need AMP, Xc, Yc, and WID.

AMP: amplitude (m) of initial  $\eta$ , if WAVEMAKER = INI\_REC, WAVEMAKER = INI\_SOL, WAVEMAKER = LEF\_SOL.

DEP: water depth at wavemaker location, if WAVEMAKER = INI\_SOL, WAVEMAKER = LEF\_SOL.

LAGTIME, time lag (s) for the solitary wave generated on the left boundary, e.g., WAVEMAKER = LEF\_SOL.

XWAVEMAKER:  $x$  (m) coordinate for WAVEMAKER = INI\_SOL.

Xc:  $x$  (m) coordinate of the center of a rectangular hump if WAVEMAKER = INI\_REC.

Yc:  $y$  (m) coordinate of the center of a rectangular hump if WAVEMAKER = INI\_REC.

WID: width (m) of a rectangular hump if WAVEMAKER = INI\_REC, or INI\_GAU.

Time\_ramp: time ramp (s) for Wei and Kirby (1999) wavemaker.

Delta\_WK: width parameter  $\delta$  for Wei and Kirby (1999) wavemaker.  $\delta = 0.3 \sim 0.6$

DEP\_WK: water depth (m) for Wei and Kirby (1999) wavemaker.

Xc\_WK:  $x$  coordinate (m) for Wei and Kirby (1999) wavemaker.

Ywidth\_WK: width (m) in  $y$  direction for Wei and Kirby (1999) wavemaker.

Tperiod: period (s) of regular wave for Wei and Kirby (1999) wavemaker.

AMP\_WK: amplitude (m) of regular wave for Wei and Kirby (1999) wavemaker.

Theta\_WK: direction (degrees) of regular wave for Wei and Kirby (1999) wavemaker. Note: it may be adjusted for a periodic boundary case by the program. A warning will be given if adjustment is made.

FreqPeak: peak frequency (1/s) for Wei and Kirby (1999) irregular wavemaker.

FreqMin: low frequency cutoff (1/s) for Wei and Kirby (1999) irregular wavemaker.

FreqMax: high frequency cutoff (1/s) for Wei and Kirby (1999) irregular wavemaker.

Hmo: Hmo (m) for Wei and Kirby (1999) irregular wavemaker.

GammaTMA, TMA parameter  $\gamma$  for Wei and Kirby (1999) irregular wavemaker.

ThetaPeak: peak direction (degrees) for Wei and Kirby (1999) irregular wavemaker.

Sigma.Theta: parameter of directional spectrum for Wei and Kirby (1999) irregular wavemaker.

#### **SPECIFICATION OF PERIODIC BOUNDARY CONDITION**

( Note: only south-north periodic condition was implemented)

PERIODIC: logical parameter for periodic boundary condition, T - periodic, F - wall boundary condition.

#### **SPECIFICATION OF SPONGE LAYER**

SPONGE\_ON: logical parameter, T - sponge layer, F - no sponge layer.

Sponge\_west\_width: width (m) of sponge layer at west boundary.

Sponge\_east\_width: width (m) of sponge layer at east boundary.

Sponge\_south\_width: width (m) of sponge layer at south boundary.

Sponge\_north\_width: width (m) of sponge layer at north boundary

R\_sponge: decay rate in sponge layer. Its values are between 0.85 ~ 0.95.

A\_sponge: maximum damping magnitude. The value is ~ 5.0.

#### **SPECIFICATION OF OBSTACLES**

OBSTACLE\_FILE: name of obstacle file. 1 - water point, 0 - permanent dry point. Data dimension is (Mglob  $\times$  Nglob). Data format is the same as the depth data.

#### **SPECIFICATION OF PHYSICS**

DISPERSION: logical parameter for inclusion of dispersion terms. T - calculate dispersion, F - no dispersion terms

Gamma1: parameter for linear dispersive terms. 1.0 - inclusion of linear dispersive terms, 0.0 - no linear dispersive terms.

Gamma2: parameter for nonlinear dispersive terms. 1.0 - inclusion of nonlinear dispersive terms, 0.0 - no nonlinear dispersive terms.

Gamma1=1.0, Gamma2=0.0 for NG's equations. Gamma1=1.0, Gamma2=1.0 for the fully nonlinear Boussinesq equations.

Gamma3: parameter for linear shallow water equations (Gamma3 = 1.0). When Gamma3 = 0.0, Gamma1 and Gamma2 automatically become zero.

Beta\_ref: parameter  $\beta$  defined for the reference level.  $\beta = -0.531$  for NG's and FUNWAVE equations.

SWE\_ETA\_DEP: ratio of height/depth for switching from Boussinesq to NSWE. The value is  $\sim 0.80$ .

### **SPECIFICATION OF FRICTION**

FRICION\_MATRIX: logical parameter for homogeneous and inhomogeneous friction field. T - inhomogeneous, F - homogeneous

FRICION\_FILE: input friction matrix file if FRICION\_MATRIX= T

Cd\_fixed: fixed bottom friction coefficient.

### **SPECIFICATION OF NUMERICS**

Time\_Scheme: stepping option, Runge\_Kutta or Predictor\_Corrector (not suggested for this version).

HIGH\_ORDER: spatial scheme option, FOURTH for the fourth-order, THIRD for the third-order, and SECOND for the second-order (not suggested for Boussinesq modeling).

CONSTRUCTION: construction method, HLL for HLL scheme, otherwise for averaging scheme.

CFL: CFL number, CFL  $\sim 0.5$ .

FroudeCap: cap for Froude number in velocity calculation for efficiency. The value could be 5  $\sim$  10.0.

MinDepth: minimum water depth (m) for wetting and drying scheme. Suggestion: MinDepth = 0.001 for lab scale and 0.01 for field scale.

MinDepthFrc: minimum water depth (m) to limit bottom friction value. Suggestion: MinDepthFrc = 0.01 for lab scale and 0.1 for field scale.

SHOW\_BREAKING: logical parameter to calculate breaking index. Note that breaking is calculated using shock wave capturing scheme. The index calculated here is based on Kennedy et al. (2000).

Cbrk1: parameter C1 in Kennedy et al. (2000).

Cbrk2: parameter C2 in Kennedy et al. (2000).

### **SPECIFICATION OF OUTPUT VARIABLES**

NumberStations: number of station for output. If NumberStations > 0, need input i,j in STATION\_FILE

DEPTH\_OUT: logical parameter for output depth. T or F.

U: logical parameter for output  $u$ . T or F.

V: logical parameter for output  $v$ . T or F.

ETA: logical parameter for output  $\eta$ . T or F.

MASK: logical parameter for output wetting-drying MASK. T or F.

MASK9: logical parameter for output MASK9 (switch for Boussinesq/NSWE). T or F.

SourceX: logical parameter for output source terms in  $x$  direction. T or F.

SourceY: logical parameter for output source terms in  $y$  direction. T or F.

P: logical parameter for output of momentum flux in  $x$  direction. T or F.

Q: logical parameter for output of momentum flux in  $y$  direction. T or F.

Fx: logical parameter for output of numerical flux F in  $x$  direction. T or F.

Fy: logical parameter for output of numerical flux F in  $y$  direction. T or F.

Gx: logical parameter for output of numerical flux G in  $x$  direction. T or F.

Gy: logical parameter for output of numerical flux G in  $y$  direction. T or F.

AGE: logical parameter for output of breaking age. T or F.

HMAX: logical parameter for output of recorded maximum surface elevation . T or F.

HMIN: logical parameter for output of recorded minimum surface elevation . T or F.

UMAX: logical parameter for output of recorded maximum velocity . T or F.

VORMAX: logical parameter for output of recorded maximum vorticity . T or F.

MFMAX: logical parameter for output of recorded maximum momentum flux . T or F.

#### 4.5.1 Specifications of Grid Inputs

All of the grid inputs such as depth file, drag coefficient matrix, and initial condition (INI\_UVZ) have the dimension Mglob x Nglob with the first point as the south-west corner. Since the read format in the code is the way that is shown below,

```
DO J=1,Nglob
  READ(1,*)(Depth(I,J),I=1,Mglob)
ENDDO
```

the input files could be generated through FORTRAN with following approach,

```
OPEN(1,file='filename.txt')
DO J=1,Nglob
  WRITE(1,100)(Depth(I,J),I=1,Mglob)
ENDDO
100 FORMAT(2000f12.3)
```

Also, in order to generate the grid inputs' input file inside MATLAB one can use the following command to generate the appropriate file,

```
dlmwrite('filename.txt',d,'\t')
```

with 'd' as the matrix(depth,drag coefficient,...) intended to be written inside the file.

#### 4.6 Input for the spherical code

All input parameters, except the following grid information, are the same as for the Cartesian code.

Lon\_West: longitude (degrees) of west boundary.

Lat\_South: latitude (degrees) of south boundary.

Dphi:  $d\phi$  (degrees)

Dtheta:  $d\theta$  (degrees)

In addition, it is not necessary to specify Gamma2 (for nonlinear dispersive terms) in the spherical code.

Another feature of the spherical code is that a computational grid can be a stretched grid. For a stretched grid, a user should set StretchGrid = T and provide grid files for DX and DY and a file for Coriolis parameters at each grid point. For example,

DX\_FILE = dx\_str.txt

DY\_FILE = dy\_str.txt

CORIOLIS\_FILE = cori\_str.txt

However, use of a stretched grid is not recommended in terms of decrease in numerical accuracy for higher order numerical schemes.

#### 4.7 Model nesting

The present version has a capability for one-way nesting. The nesting scheme passes surface elevation and velocity components calculated from a large domain to a nested small domain through ghost cells at nesting boundaries. To run a nested model, the following procedures should be performed.

1. The coupling option in Makefile should be defined as '-Dcoupling'. The program should be re-compiled.
2. Prepare nesting data using the output of a large-domain model. The following is an example of the data format.

coupling data

boundary info: num of points (negative means no point), start point

EAST

-1 1 (*no data on east side*)

WEST

5 1 (*5 points at west boundary, start from 1*)

SOUTH

-1 0 (*no data on south side*)

NORTH

-1 0 (*no data on north side*)

TIME SERIES

68.443001 (*first step, NOTE: model clock will be initialized as this time*)

EAST SIDE (*no nesting on east side*)

WEST SIDE

0.141220E-02 0.141220E-02 0.141220E-02 0.141220E-02 0.141220E-02 (*u*)

-0.119260E-10 -0.119260E-10 -0.667390E-10 -0.667390E-10 -0.219240E-10 (*v*)

```

0.141890E-02 0.141890E-02 0.141890E-02 0.141890E-02 0.141890E-02 (z)
SOUTH SIDE (no nesting on south side)
NORTH SIDE (no nesting on north side)
68.641998 (next time step)
...

```

The example above is a case that a model nesting takes place at the WEST (left) boundary of a small domain. Boundaries are defined with the order: EAST, WEST, SOUTH, and NORTH. If the num of points of a boundary is larger than zero, the program will read a time series of  $(u, v, \eta)$  below 'XXXX SIDE'. The read format is

```

READ(11,*) TIME_COUPLING_2
READ(11,119)(U_COUPLING_EAST(I,2),I=1,N_COUPLING_EAST)
READ(11,119)(V_COUPLING_EAST(I,2),I=1,N_COUPLING_EAST)
READ(11,119)(Z_COUPLING_EAST(I,2),I=1,N_COUPLING_EAST)
ENDDO
119 FORMAT(5E16.6)

```

where N\_COUPLING\_EAST is Num of points at the EAST boundary.

3. Specify the file of coupling data in input.txt

```

! _____ COUPLING _____
! if do coupling, have to set -DCOUPLING in Makefile
COUPLING_FILE = coupling.txt
where 'coupling.txt' is the file saved in procedure 2.

```

## 4.8 Output

The output files are saved in the result directory defined by RESULT\_FOLDER in input.txt. For outputs in ASCII, a file name is a combination of variable name and an output series number such eta\_0001, eta\_0002, .... The format and read/write algorithm are consistent with a depth file. Output for stations is a series of numbered files such as sta\_0001, sta\_0002 ....

The NetCDF output format is under development.

## 5 Examples

The model has been validated extensively using laboratory experiments for wave shoaling and breaking as in the FUNWAVE manual by Kirby et al. (1998). In addition, Tehranirad et al. (2011) used FUNWAVE-TVD Version 1.0 to carry out tsunami benchmark testing in conjunction with the National Tsunami Hazard Mitigation Program. Tests of mass conservation and convergence are included in Tehranirad et al. (2011).

## 5.1 Breaking waves on a beach

Hansen and Svendsen (1979) carried out laboratory experiments of wave shoaling and breaking on a beach. Waves were generated on a flat bottom a 0.36 m depth, and the beach slope was 1:34.26. The experiments included several cases including plunging breakers, plunging-spilling breakers and spilling breakers. In this paper, we simulate two typical cases: a plunging breaker and a spilling breaker, respectively. The wave height and wave period are 4.3 cm and 3.33 s, respectively, for the plunging case, and 6.7 cm and 1.67 s for the spilling case.

Although the shock-capturing breaking algorithm used in Boussinesq wave models has been examined by previous researchers (e.g., Tonelli and Petti, 2009, Shiach and Mingham, 2009 and others), there is a concern about its sensitivity to grid spacing. In this study, we adopted three grid sizes,  $dx = 0.05$  m, 0.025 m and 0.0125 m, respectively, for each cases. Figure 3 shows comparisons of wave height and wave setup between measured data and numerical results from model runs with different grid sizes. The wave breaking location of wave setup/setdown predicted by the three runs are in agreement with the data, however, the predicted maximum wave heights are slightly different. Results from the  $dx=0.25$  m and 0.0125 m grids are very close, indicating a convergence with grid refinement. All three models underpredict the peak wave height at breaking and overpredict wave height inside of the surfzone. This prediction trend was also found in Kennedy et al. (2000, Figure 2). About 10% underprediction of peak wave height can be found in our tests with  $dx = 0.025$  m and 0.0125 m, which is similar to Kennedy et al. (2000). The model with a coarser grid ( $dx = 0.05$  m) underpredicted the maximum wave height by 20%.

To find the cause of the large underprediction of peak wave height in the coarser grid model, in Figure 4, we show snapshots of surface elevation from model results with  $dx = 0.025$  m and 0.050 m at different times. The model with the finer grid resolution switched from the Boussinesq equations to NSWSE around  $t = 19.9$ s (the model with the coarser grid switched slightly later) at the point where the ratio of surface elevation to water depth reached the threshold value of 0.8. Then, a wave is damped at the sharp front and generates trailing high frequency oscillations. The comparison of wave profiles at an early time (i.e.  $t = 18.6$  s) shows that the coarser grid model underpredicts wave height before the Boussinesq-NSWE switching, indicating that the underprediction is not caused by the shock-capturing scheme, but by the numerical dissipation resulting from the coarse grid resolution.

For the spilling breaker case, the models with three different grid sizes basically predicted slightly different wave peaks as in the plunging wave case. Figure 5 shows results with  $dx = 0.25$  m, where the model provides very good predictions of wave shoaling to near the breaking limit. Once again, the model overpredicts wave height inside the surf zone.

Some necessary definitions in the input file, input.txt, for the plunging breaker case are

```
! -----DEPTH-----  
DEPTH _TYPE = SLOPE  
DEPTH _FLAT = 0.36  
SLP = 0.0292
```

```

Xslp = 55.0
! -----DIMENSION-----
Mglob = 3001
Nglob = 3
! ----- TIME -----
DX = 0.025
DY = 0.2 ! give any larger value than DX for 1-D case
! -----WAVEMAKER-----
WAVEMAKER = WK _REG
Xc _WK = 45.0
Tperiod = 3.33
AMP _WK = 0.0185
DEP _WK = 0.36
Theta _WK = 0.0
Time _ramp = 1.0
Delta _WK = 0.3
! ----- SPONGE LAYER -----
SPONGE _ON = T
Sponge _west _width = 10.0
Sponge _east _width = 0.0
Sponge _south _width = 0.0
Sponge _north _width = 0.0
R _sponge = 0.95
A _sponge = 5.0
! -----PHYSICS-----
DISPERSION = T
Gamma1 = 1.0
Gamma2 = 1.0
Gamma3=1.0
Beta _ref=-0.531
SWE _ETA _DEP = 0.8
Cd = 0.0 ! Cd is not sensitive for this case
! -----NUMERICS-----
Time _Scheme = Runge _Kutta
HIGH _ORDER = FOURTH
CONSTRUCTION = HLLC
CFL = 0.5
! -----WET-DRY-----
MinDepth=0.001
MinDepthFrc = 0.001
! -----OUTPUT-----

```

DEPTH\_OUT = T  
 ETA = T  
 MASK = T

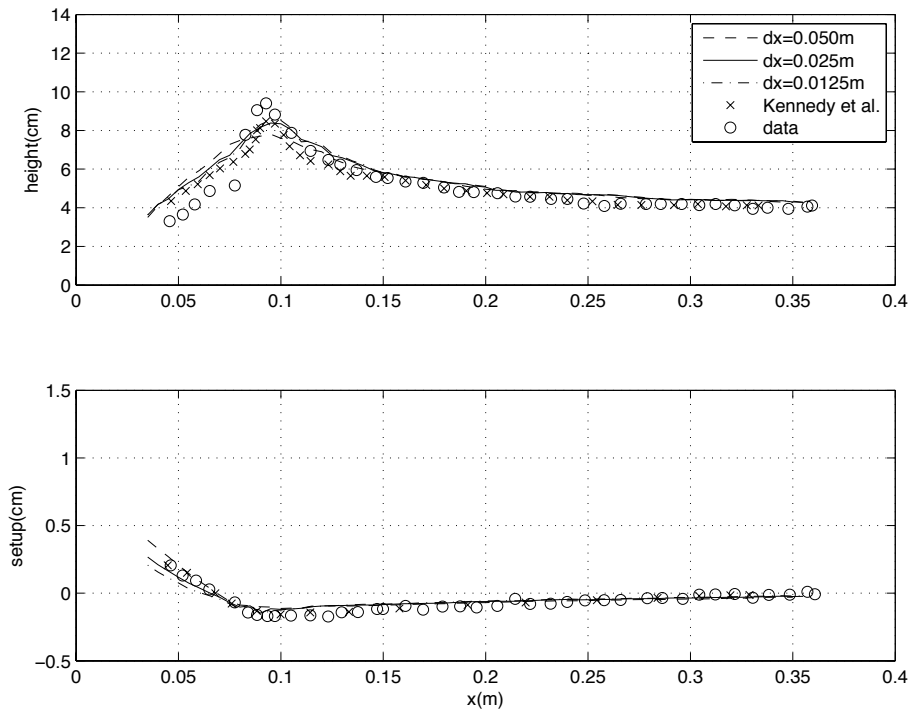


Figure 3: Comparisons of wave height (upper panel) and wave setup (lower panel) between measured data and model results from grid resolutions of  $dx = 0.0125$  m,  $0.025$  m and  $0.050$  m, respectively. Case: plunging breaker.

## 5.2 Random wave shoaling and breaking on a slope (in directory /mase\_kirby\_1d/)

To study random-wave properties of shoaling and breaking, Mase and Kirby (1992) conducted a laboratory experiment of random wave propagation over a planar beach. The experiment layout is shown in Figure 6, where a constant depth of  $0.47$  m on the left connects to a constant slope of  $1:20$  on the right. Two sets of random waves with peak frequencies of  $0.6$  Hz (run 1) and  $1.0$  Hz (run 2) were generated by the wavemaker on the left. The target incident spectrum was a Pierson-Moskowitz spectrum. Wave gauges at depths  $h = 47, 35, 30, 25, 20, 17.5, 15, 12.5, 10, 7.5, 5,$  and  $2.5$  cm collected time series of surface elevation.

Wei and Kirby (1995) carried out a simulation of run 2 without wave breaking. Later, Kirby et al. (1998) and Kennedy et al. (2000) carried out the same simulation with wave breaking. The

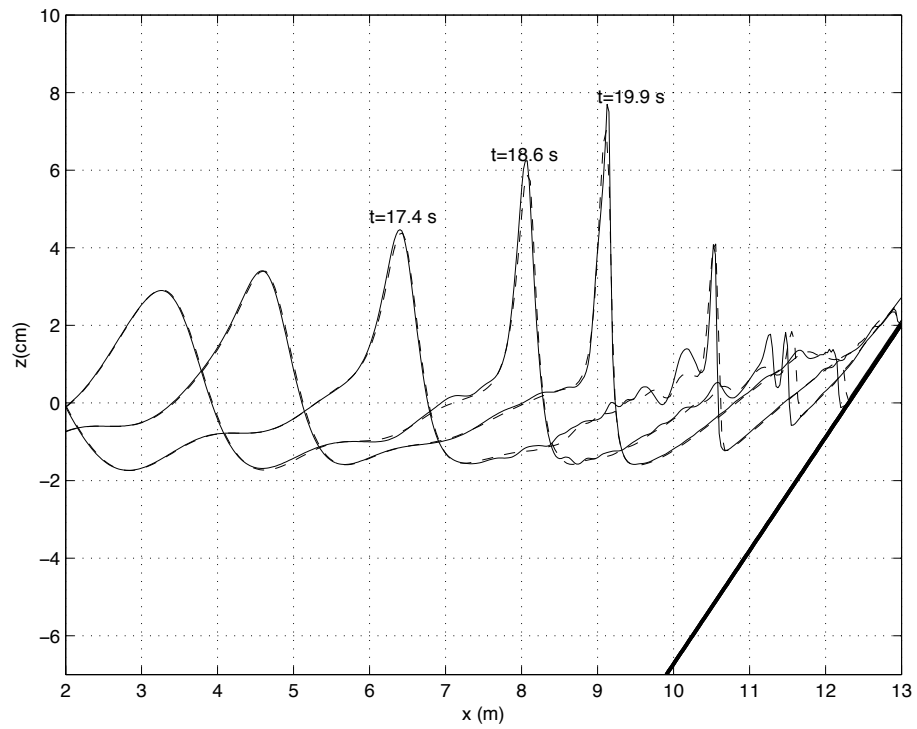


Figure 4: Snapshots of surface elevation at  $t = 17.4$ ,  $18.6$  and  $19.9$  s from models with grid resolutions of  $dx = 0.025$  (solid lines) and  $0.050$  m (dashed lines).

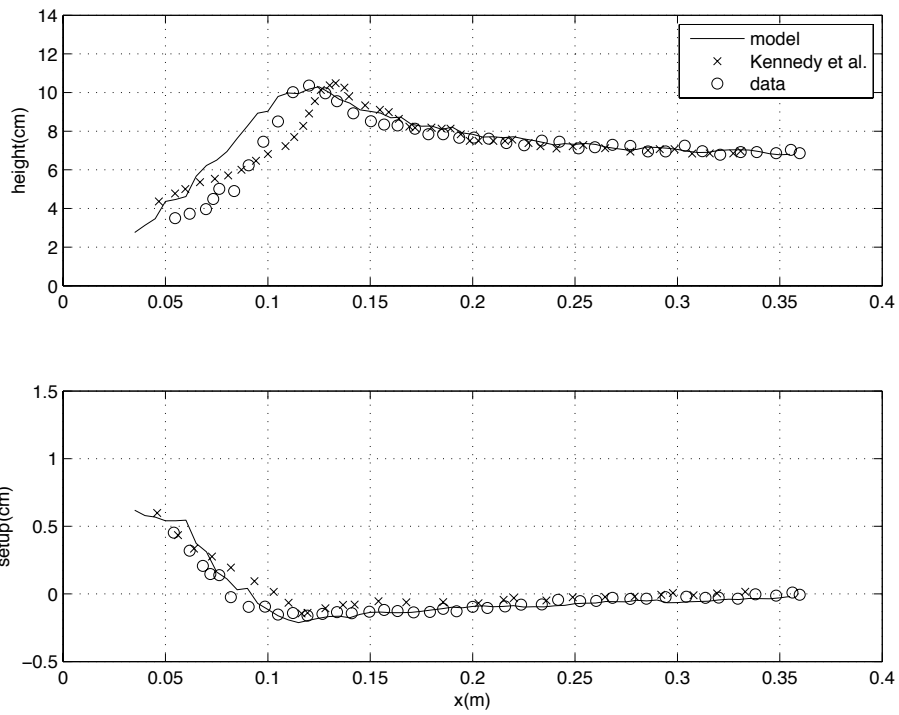


Figure 5: Model/data comparisons of wave height (upper panel) and wave setup ( $dx = 0.025$  m). Case: spilling breaker.

present model was set up following Kirby et al. (1998), who used an internal wavemaker located at the toe of the slope where surface elevation is measured (gauge 1).

A *FFT* was used to transform between the time domain and frequency domain data required by the wavemaker. A MATLAB script, (*fft4wavemaker.m*) to perform this transform is included in the example. The script reads the measured data from the file called *r2d470.dat*, and saves calculated wave amplitude, period and phase information for each component in the file named as *wavemk\_per\_amp pha.txt*. The low and high-frequency cutoffs are 0.2 and 10.0 Hz, respectively.

The simulation time is the same as the time length of data collection. The computational domain is from  $x = 0$  m to 20 m with a grid size of 0.04 m. The toe of the slope starts at  $x = 10$  m. A sponge layer is specified at the left side boundary, to absorb reflected waves, but no sponge layer is needed on the right boundary, which differs from Kirby et al. (1998) who used the slot method combined with a sponge layer at the end of the domain.

We present the model results for run 2 and compare with the experimental data measured at the other 11 gauges shown in Figure 6. Figure 7 shows model results (dashed lines) and measured data (solid lines) from  $t = 20$  s to  $t = 40$  s at those gauges. Both model and data show that most waves start breaking at the depth  $h = 15$  cm. Except for small discrepancies for wave phases, the model reproduces the measured waveform quite well.

To further demonstrate the applicability of the model, we performed third moment computations of the resulting time series of surface elevation. Normalized wave skewness and asymmetry were calculated for both measured and modeled time series of surface elevation according to the following formulations,

$$\begin{aligned} \text{skew} &= \frac{\langle \eta^3 \rangle}{\langle \eta^2 \rangle^{3/2}} \\ \text{asym} &= \frac{\langle H(\eta)^3 \rangle}{\langle \eta^2 \rangle^{3/2}} \end{aligned} \quad (79)$$

where  $H$  denotes the Hilbert transform,  $\langle \rangle$  is the mean operator, and the mean has been removed from the time series of surface elevation.

Figure 8 shows the comparisons of skewness and asymmetry between the model results and experiment data. The model predicted skewness and asymmetry reasonably well with a slightly overprediction of wave skewness inside the surf zone.

It is worth mentioning that Kirby et al. (1998) employed more frequent use of numerical filtering, especially after wave breaking, so that the model run was stable over the entire data time series. The present model did not encounter any stability problem without filtering.

Some necessary definitions in the input file, *input.txt*, are

```
! _____DEPTH_____
DEPTH_TYPE = SLOPE
DEPTH_FLAT = 0.47
SLP = 0.05
```

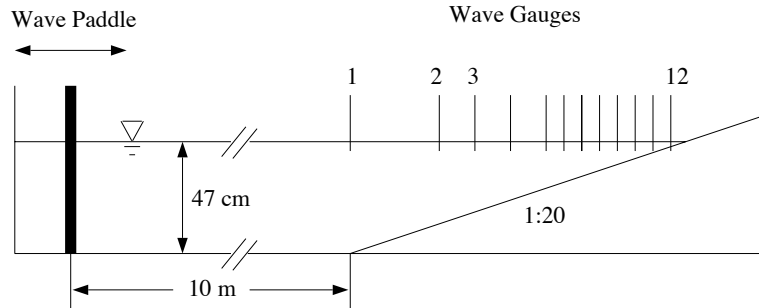


Figure 6: Experiment layout of Mase and Kirby (1992).

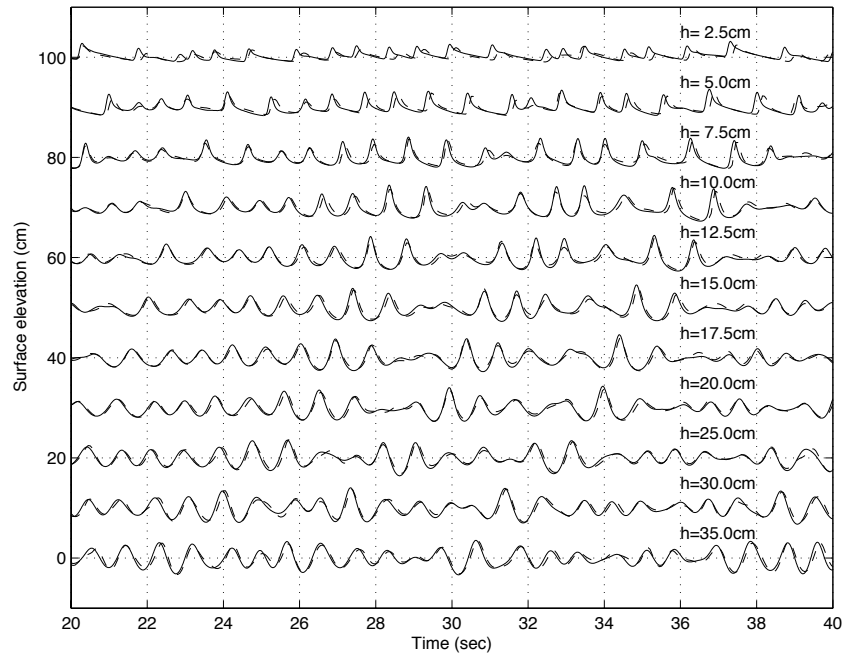


Figure 7: Time series comparison of  $\eta$  between model (dashed lines) and data (solid lines) at 11 wave gauges in Mase and Kirby (1992).

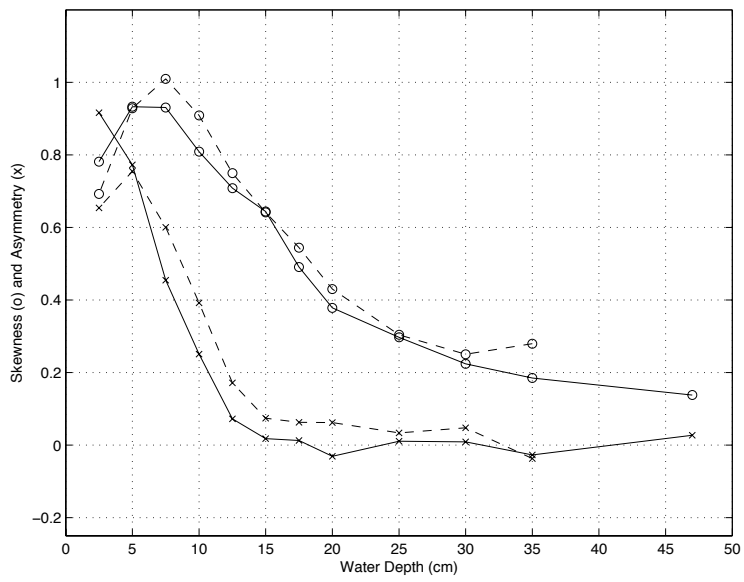


Figure 8: Comparison of skewness (o) and asymmetry (x) at different water depths. Solid lines are experiment data (Mase and Kirby, 1992). Dashed lines are numerical results

Xslp = 10.0

! -----DIMENSION-----

Mglob = 500

Nglob = 3

! -----TIME-----

TOTAL\_TIME = 716.0

PLOT\_INTV = 10.0

PLOT\_INTV\_STATION = 0.05

SCREEN\_INTV = 1.0

! -----GRID-----

DX = 0.04

DY = 0.10

! -----WAVEMAKER-----

WAVEMAKER = WK\_TIME\_SERIES

NumWaveComp = 1505

PeakPeriod = 1.0

WaveCompFile = ../fft/wavemk\_per\_amp\_pha.txt

! Wei and Kirby 1999

Time\_ramp = 1.0

Delta\_WK = 0.4 ! width parameter 0.3-0.6

DEP\_WK = 0.47

Xc\_WK = 10.0

Ywidth\_WK = 10000.0 ! give any bigger value than the width of tank

! -----SPONGE LAYER-----

SPONGE\_ON = T

Sponge\_west\_width = 2.0

Sponge\_east\_width = 0.0

Sponge\_south\_width = 0.0

Sponge\_north\_width = 0.0

R\_sponge = 0.90

A\_sponge = 5.0

! -----PHYSICS-----

DISPERSION = T

Gamma1 = 1.0

Gamma2 = 1.0

Gamma3 = 1.0  
Beta\_ref=-0.531  
SWE\_ETA\_DEP = 0.80  
Cd = 0.001 ! not sensitive for this case

```
! -----NUMERICS-----  
Time_Scheme = Runge_Kutta  
HIGH_ORDER = FOURTH  
CONSTRUCTION = HLLC  
CFL = 0.5  
! -----WET-DRY-----  
MinDepth=0.001  
MinDepthFrc = 0.001  
! -----OUTPUT-----  
NumberStations = 12  
STATIONS_FILE = gauges_004.txt  
DEPTH_OUT = T  
ETA = T
```

Model output at 12 gauges are saved in *sta\_0001*, *sta\_0002*, ..., *sta\_0012*. Use MATLAB scripts, *comp\_mksskew.m* and *cmop\_series.m* for plots.

### 5.3 Wave propagation over a shoal: Berkhoff et al. (1982) (in directory /berkhoff\_2d/)

The laboratory experiment of wave propagation over a shoal conducted by Berkhoff et al. (1982) has served as a standard test for examining numerical model performances in predicting wave shoaling, refraction, diffraction and nonlinear dispersion. Kirby et al. (1998) showed that the previous version of FUNWAVE accurately reproduces measured wave heights in the experiments. Here, in this manual, we repeat this test exactly following Kirby et al. (1998).

The bottom topography is shown in Figure 9, which is generated using the same program in Kirby et al., (1998). The topography consists of an elliptic shoal resting on a plane beach with a constant slope 1/50. Bottom contours on the slope are oriented at an angle of  $20^\circ$  to the  $y$  axis. Regular waves with period of 1s and amplitude of 2.32cm are generated by a wavemaker at  $x = -10m$  and propagate across the domain. Experiment data are collected along 8 transects as shown in the figure. Two vertical side walls are located at  $y = -10m$  and  $y = 10m$ . Detailed information on the geometry may be obtained in Berkhoff et al. (1982) or Kirby and Dalrymple (1984).

The computational domain used in the model is the same as in Figure 9 except for two sponge layers with a width of 2m sitting behind wavemaker and on the end of the beach. The source function for generating the corresponding monochromatic wave is located at the wavemaker.

Thirty waves are simulated in order to get a quasi-stable wave condition. The time series of

surface elevation in the last 5 seconds (5 wave periods) are used for the wave height estimation at each grid point. Matlab post-processing scripts, *calcheight.m* and *showheight.m* are provided in the example. Figure 10 shows comparisons between model results and experimental data along the eight transects where measurements were made. The model results of wave height agree well with experimental data, in both sections parallel or normal to incident wave direction. The results from the present model are also similar to that from the previous version of FUNWAVE in Kirby et al. (1998).

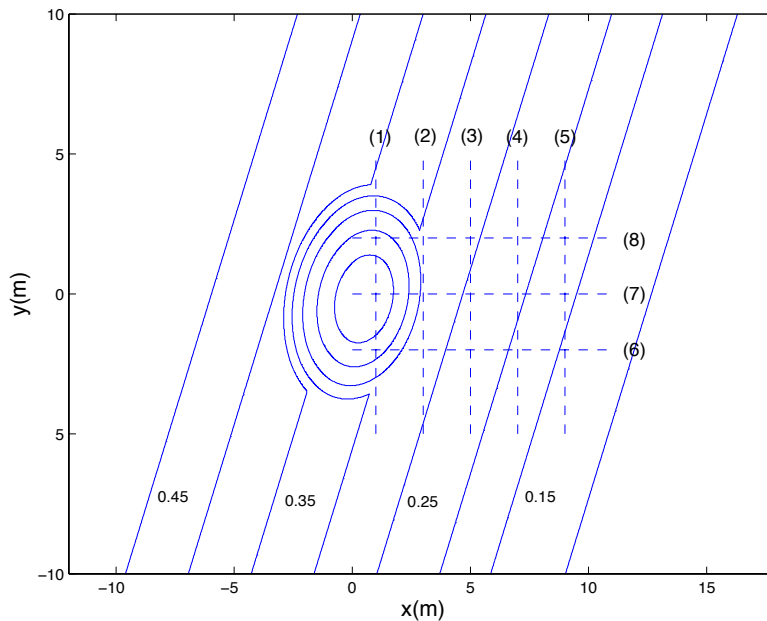


Figure 9: Experiment layout for wave focusing experiment of Berkhoff et al. (1982).

Parameters and other definitions specified in *input.txt* are listed below.

```
! _____DEPTH_____
DEPTH_TYPE = DATA
DEPTH_FILE = ../input/depth.txt

! _____DIMENSION_____
Mglob = 600
Nglob = 200

! _____TIME_____
```

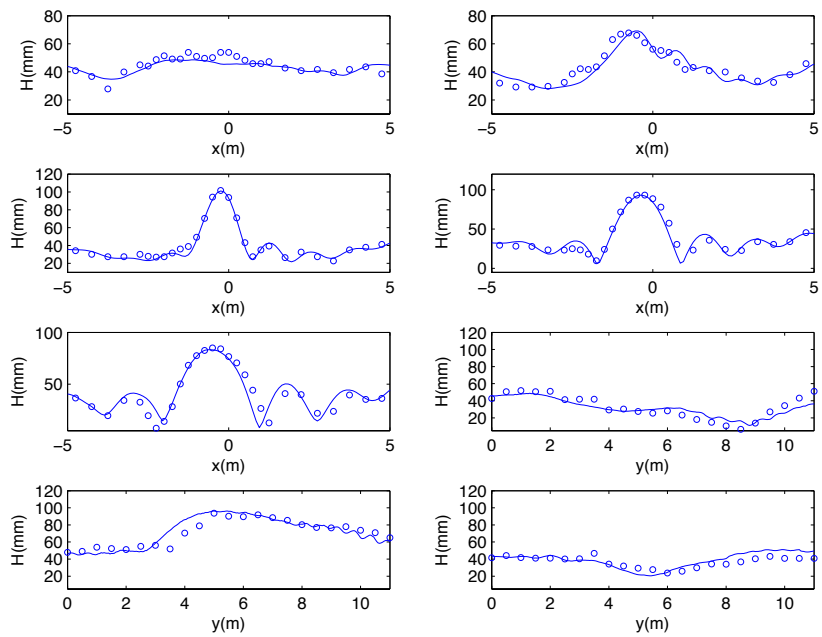


Figure 10: Comparisons of wave height along specified sections between the model (solid lines) and experiment data (circles).

TOTAL\_TIME = 30.0  
PLOT\_INTV = 0.02  
PLOT\_INTV\_STATION = 0.02  
SCREEN\_INTV = 0.1

! -----GRID-----

DX = 0.05  
DY = 0.10

! -----WAVEMAKER-----

WAVEMAKER = WK\_REG  
Time\_ramp = 1.0  
Delta\_WK = 0.5 ! width parameter 0.3-0.6  
DEP\_WK = 0.45  
Xc\_WK = 3.0  
Ywidth\_WK = 10000.0 ! give any larger value than the width of flume  
Tperiod = 1.0  
AMP\_WK = 0.0232  
Theta\_WK = 0.0

! -----SPONGE LAYER-----

SPONGE\_ON = T  
Sponge\_west\_width = 2.0  
Sponge\_east\_width = 2.0  
Sponge\_south\_width = 0.0  
Sponge\_north\_width = 0.0  
R\_sponge = 0.90  
A\_sponge = 5.0

! -----PHYSICS-----

DISPERSION = T  
Gamma1 = 1.0  
Gamma2 = 1.0  
Gamma3 = 1.0  
Beta\_ref = -0.531  
SWE\_ETA\_DEP = 0.80  
Cd = 0.0

! -----NUMERICS-----

Time\_Scheme = Runge\_Kutta  
HIGH\_ORDER = FOURTH

```
CONSTRUCTION = HLLC
CFL = 0.5
```

```
! _____WET-DRY_____
MinDepth=0.001
MinDepthFrc = 0.001
```

```
! _____OUTPUT_____
NumberStations = 0
DEPTH_OUT = T
ETA = T
```

#### 5.4 Solitary wave on a conical island

Laboratory experiments on the interaction between solitary waves and a conical island were conducted by Briggs et al (1995). The three cases from this test illustrate the important fact that runup and inundation heights on the sheltered back sides of an island can exceed the incident wave height on the exposed front side, due to trapping of wave fronts propagating around the island circumference. These tests have been used in a number of validation studies for a variety of models, including nonlinear shallow water equations (Liu et al 1995) and Boussinesq equations (Chen et al, 2000). The benchmark test is specified in Section 3.3 of Appendix A of Synolakis et al (2007).

Large-scale laboratory experiments were performed at Coastal Engineering Research Center, Vicksburg, Mississippi, in a 30m-wide, 25m-long, and 60cm-deep wave basin (Figure 11). In the physical model, a 62.5cm-high, 7.2m toe-diameter, and 2.2m crest-diameter circular island with a 1:4 slope was located in the basin (Figure 12). Experiments were conducted at depth of 32cm, with three different solitary waves ( $H/d=0.045, 0.091, 0.181$ ). Water-surface time histories were measured with 27 wave gages located around the perimeter of the island (Figure 13).

For this benchmark test, time histories of the surface elevation around the circular island are given at four locations, i.e., in the front of the island at the toe (Gauge 6) and gauges closest to the shoreline with the numbers 9, 16, and 22 located at the  $0^\circ, 90^\circ,$  and  $180^\circ$  radial lines (Figure 13). A grid size of  $\Delta x = 0.05m$  is considered for proper numerical simulation of this benchmark. Figures 14-16 shows the comparison between the laboratory data with numerical calculations. Table 1 represents the error of the maximum runup for each gauge for different wave heights.

Input parameters in the tests are listed as below.

```
! _____DEPTH_____
DEPTH_TYPE = DATA
DEPTH_FILE = ../input/depth.txt
```

```
! _____DIMENSION_____
```

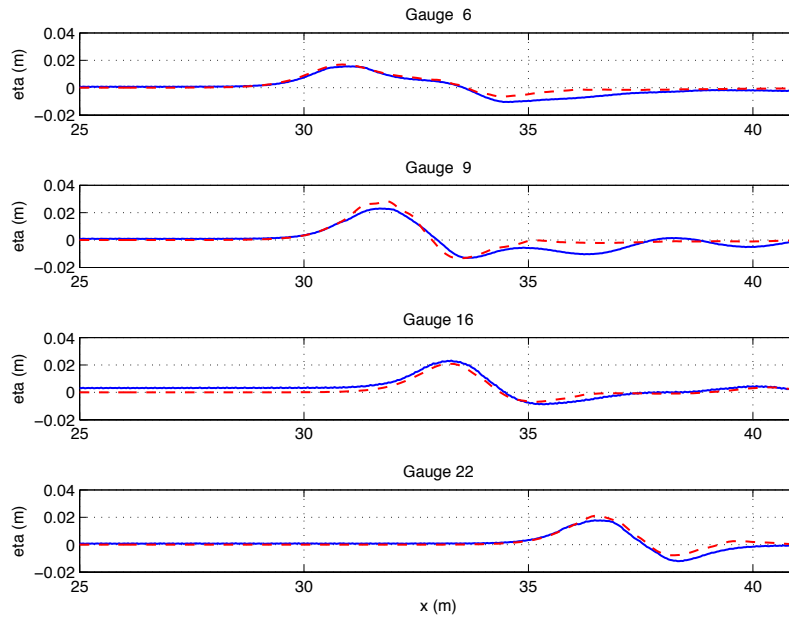


Figure 11: View of conical island(top) and basin(bottom)(from Synolakis et al (2007, Figure A16)).

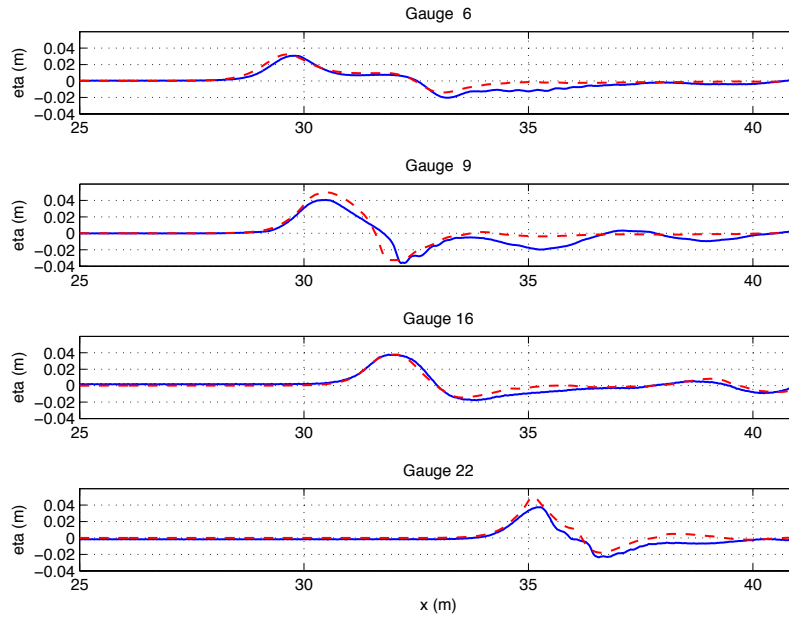


Figure 12: Definition sketch for conical island. All dimensions are in cm (from Synolakis et al (2007, Figure A17)).

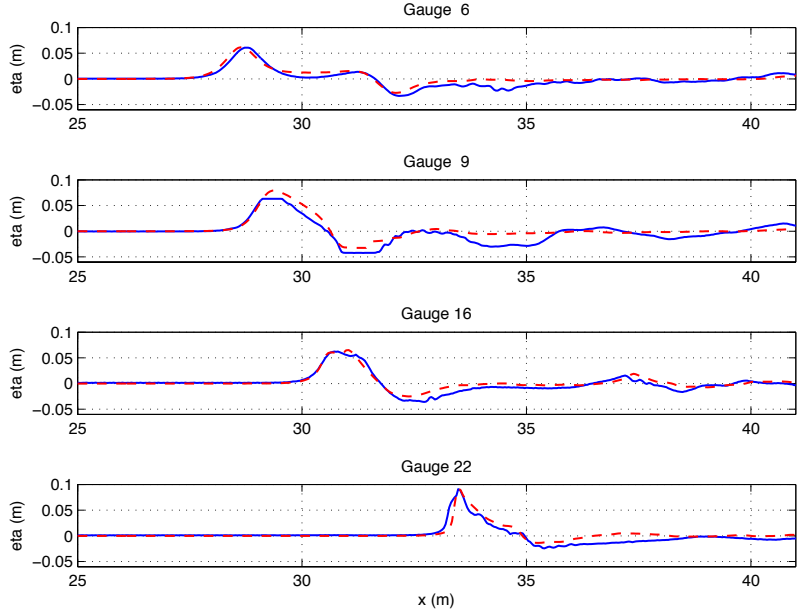


Figure 13: Schematic gauge locations around the conical island (from Synolakis et al (2007, Figure A18)).

$H/d$	Gauge Number			
	6	9	16	22
0.045	6.0	13.2	0.1	18.9
0.091	3.2	16.6	11.6	0.26
0.181	1.6	13.33	13.8	13.3

Table 1: Percent error of predicted maximum runup calculated for each gauge in conical island test.

Mglob = 702

Nglob = 602

! ———— TIME ————  
TOTAL\_TIME = 25.0  
PLOT\_INTV = 1.0  
PLOT\_INTV\_STATION = 0.05  
SCREEN\_INTV = 1.0

! ———— GRID ————  
DX = 0.05  
DY = 0.05

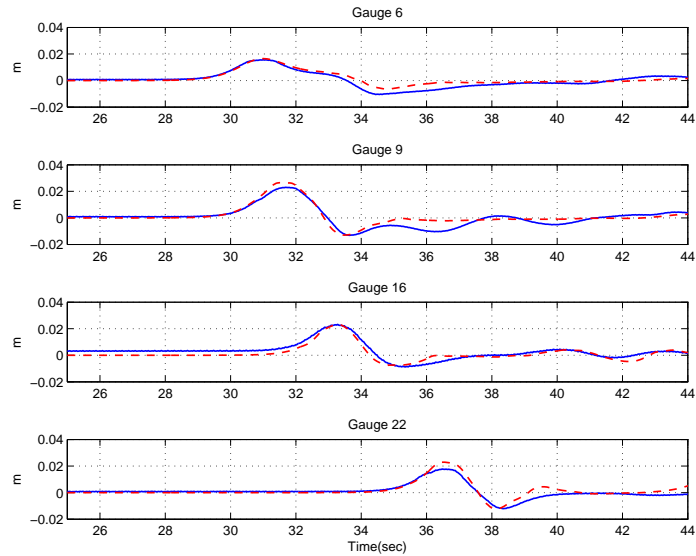


Figure 14: Comparison of computed and measured time series of free surface for  $H/d = 0.045$ . Solid lines: measured, Dashed lines: Computed.

```

! -----WAVEMAKER-----
WAVEMAKER = INI_SOL
AMP = 0.0144 ! 0.02912 for case B and 0.05792 for case C
DEP = 0.32
LAGTIME = 5.0
XWAVEMAKER = 8.0

! ----- SPONGE LAYER -----
SPONGE_ON = F

! -----PHYSICS-----
DISPERSION = T
Gamma1 = 1.0
Gamma2 = 1.0
Gamma3 = 1.0
Beta_ref=-0.531
SWE_ETA_DEP = 0.80
Cd = 0.01 ! note: not sensitive, could give a small value like 0.001

```

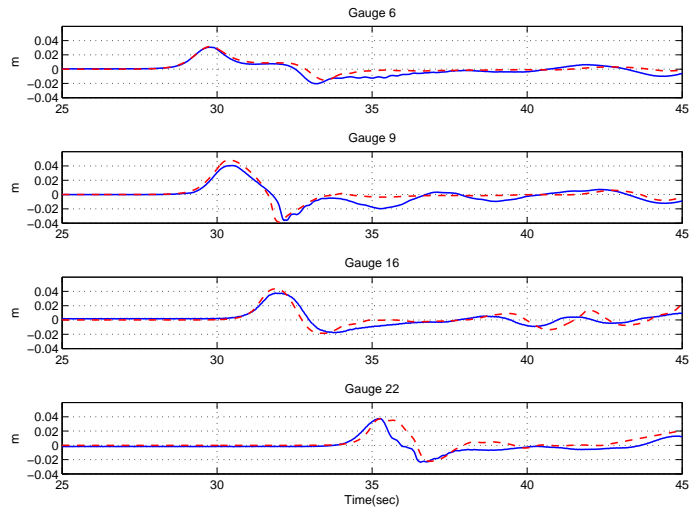


Figure 15: Comparison of computed and measured time series of free surface for  $H/d = 0.091$ . Solid lines: measured, Dashed lines: Computed.

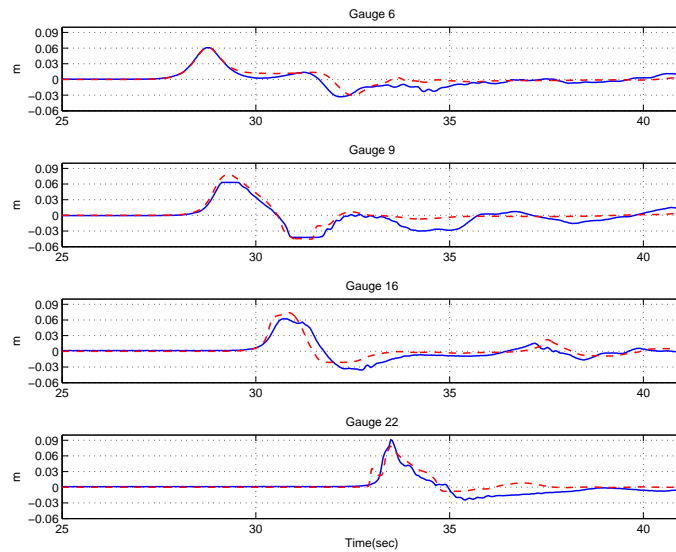


Figure 16: Comparison of computed and measured time series of free surface for  $H/d = 0.181$ . Solid lines: measured, Dashed lines: Computed.

```

! -----NUMERICS-----
Time_Scheme = Runge_Kutta
HIGH_ORDER = FOURTH
CONSTRUCTION = HLLC
CFL = 0.5

! -----WET-DRY-----
MinDepth=0.001
MinDepthFrc = 0.001

! -----OUTPUT-----
NumberStations = 16
STATIONS_FILE = gauges.txt
DEPTH_OUT = T
ETA = T
Hmax = T
MASK = T

```

The results of surface elevation at seven gauges are saved as sta\_0001 ... sta\_0016 as specified in input.txt. Model/data comparisons are carried out at sta\_0001 (gauge 6), sta\_0002 (gauge 9), sta\_0008 (gauge 16), sta\_0022 (gauge 22). A post-processing MATLAB script called *plot\_comparison.m* can be used for model/data comparisons.

## 5.5 Solitary wave runup on a shelf with an island (in directory /solitary\_runup\_2d)

In this test, we performed a simulation of the solitary wave runup measured recently in a large wave basin at Oregon State University's O.H. Hinsdale Wave Research Laboratory. The basin is 48.8 m long, 26.5 m wide, and 2.1 m deep. A complex bathymetry has been constructed, which consists of a 1:30 slope planar beach connected to a triangle shaped shelf and a conical island on the shelf as shown in Figure 17. Solitary waves were generated on the left side by a piston-type wavemaker. Surface elevation and velocity were collected at many locations by wave gauges and ADV's in alongshore and cross-shore arrays (See Swigler and Lynett, 2011 for details). Figure 17 shows wave gauges (circles) and ADV's (triangles) used for model/data comparisons in the present study. Gauge 1 - 9 were located at  $(x, y) = (7.5, 0.0), (13.0, 0.0), (21.0, 0.0), (7.5, 5.0), (13.0, 5.0), (21.0, 5.0), (25.0, 0.0), (25.0, 5.0)$  and  $(25.0, 10.0)$ , respectively. ADV 1 - 3 were located at  $(13.0, 0.0), (21.0, 0.0)$  and  $(21.0, -5.0)$ , respectively.

The modeled bathymetry was constructed by combining the measured data of the shelf and the analytical equation of the cone, which was used for the design of the island in the experiment. The computational domain was modified by extending the domain from  $x = 0.0$  m to  $-5.0$  m with a constant water depth of 0.78 m in order to use a solitary wave solution as an initial condition. The

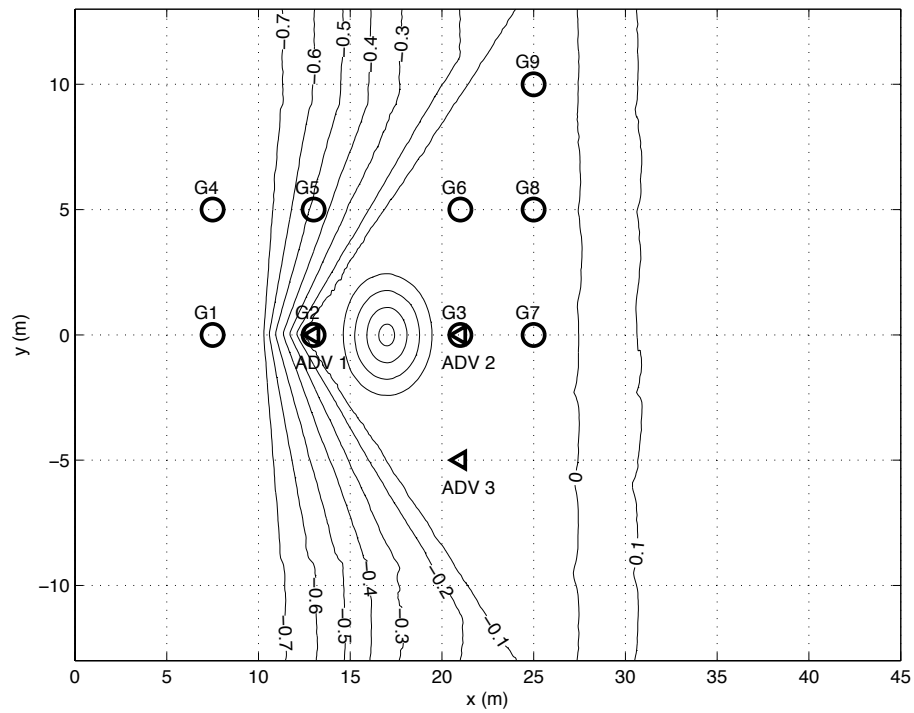


Figure 17: Bathymetry contours (in meters) and measurement locations used in model/data comparisons. Circles: pressure gauges, triangles: ADV.

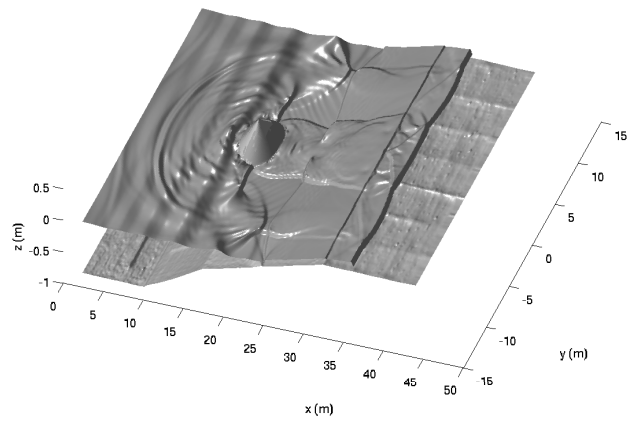
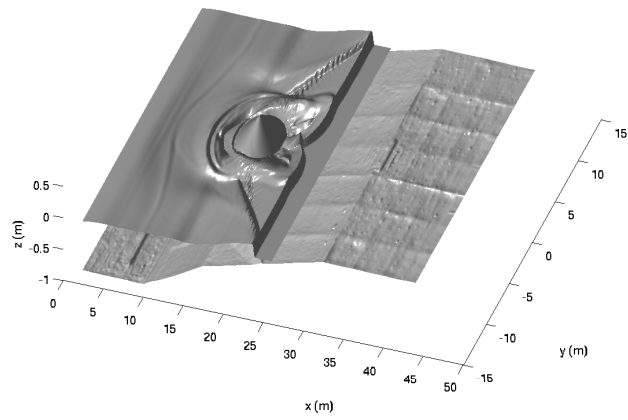
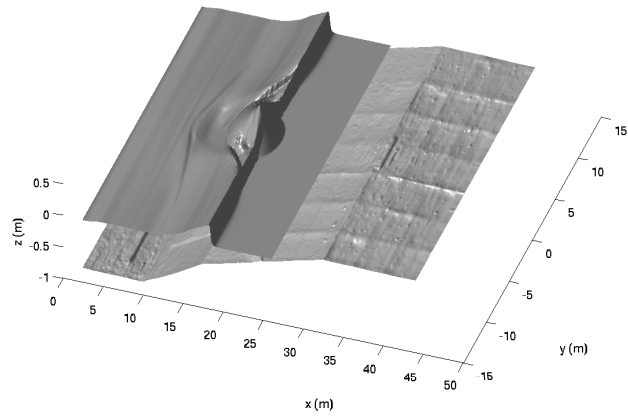


Figure 18: Modeled water surface at (top)  $t = 6.4$  s, (middle)  $t = 8.4$  s, (bottom)  $t = 14.4$  s.

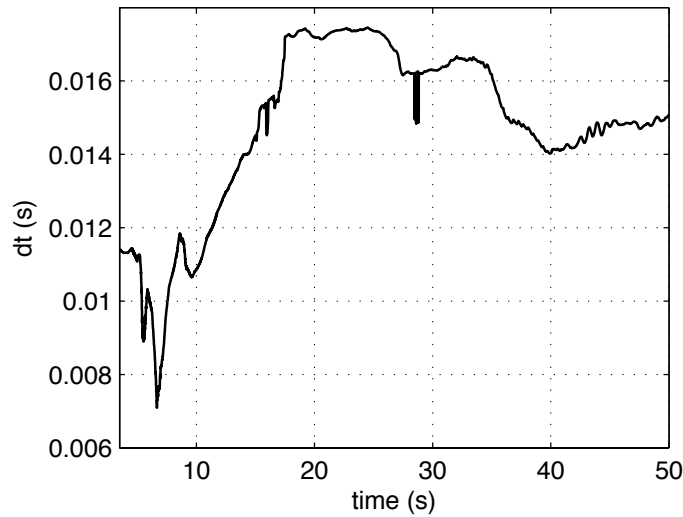


Figure 19: Time step variation.

width of the computational domain in the  $y$  direction is the same as OSU's basin. Grid spacing used in the model is 0.1 m in both directions. A solitary wave solution based on Nwogu's extended Boussinesq equations was used with centroid located at  $x = 5.0$ . The wave height is 0.39 m as that used in the laboratory experiment.

Figure 18 shows results of computed water surfaces at  $t = 6.4$  s, 8.4 s and 14.4 s, respectively. The wave front becomes very steep as the wave climbs on the shelf, which was well captured by the model. The wave scattering pattern is clearly seen in the bottom panel of Figure 18. Wave breaking on the shelf was observed in the laboratory experiment and was also seen in the model. Figure 19 shows the variation in time stepping during the simulation. The time step dropped to a minimum, at around  $t = 6.5$  s, as the wave collided with the island (top panel of figure 18). The local Froude number reached a maximum at  $t = 6.5$  s, reducing the value of the time step based on (42).

Figure 20 shows time series of modeled surface elevations and measurements at Gauge 1 - 9 (from top to bottom). Good agreement between model and data is found at the gauge in front of the island (Gauge 1, top panel), as the model successfully predicts the solitary wave propagation and its reflection from the shore. The model also captures the collision of edge waves propagating around the two sides of the island, as indicated at the gauge behind the island (Gauge 3). The model predicts the timing of wave collision well but over-predicts the peak of wave runup. The model/data comparisons at Gauges 5, 6, 8, and 9, which are located at the north-side shelf, indicates that the model predicts wave refraction and breaking on the shelf reasonably well.

Figure 21 shows model/data comparisons of velocity time series of velocity  $u$  component at ADV 1 (top panel), ADV 2 (second panel), ADV 3 (third panel), and  $v$  component at ADV 3 (bottom panel). The model predicts the peak velocity and the entire trend of velocity variation in

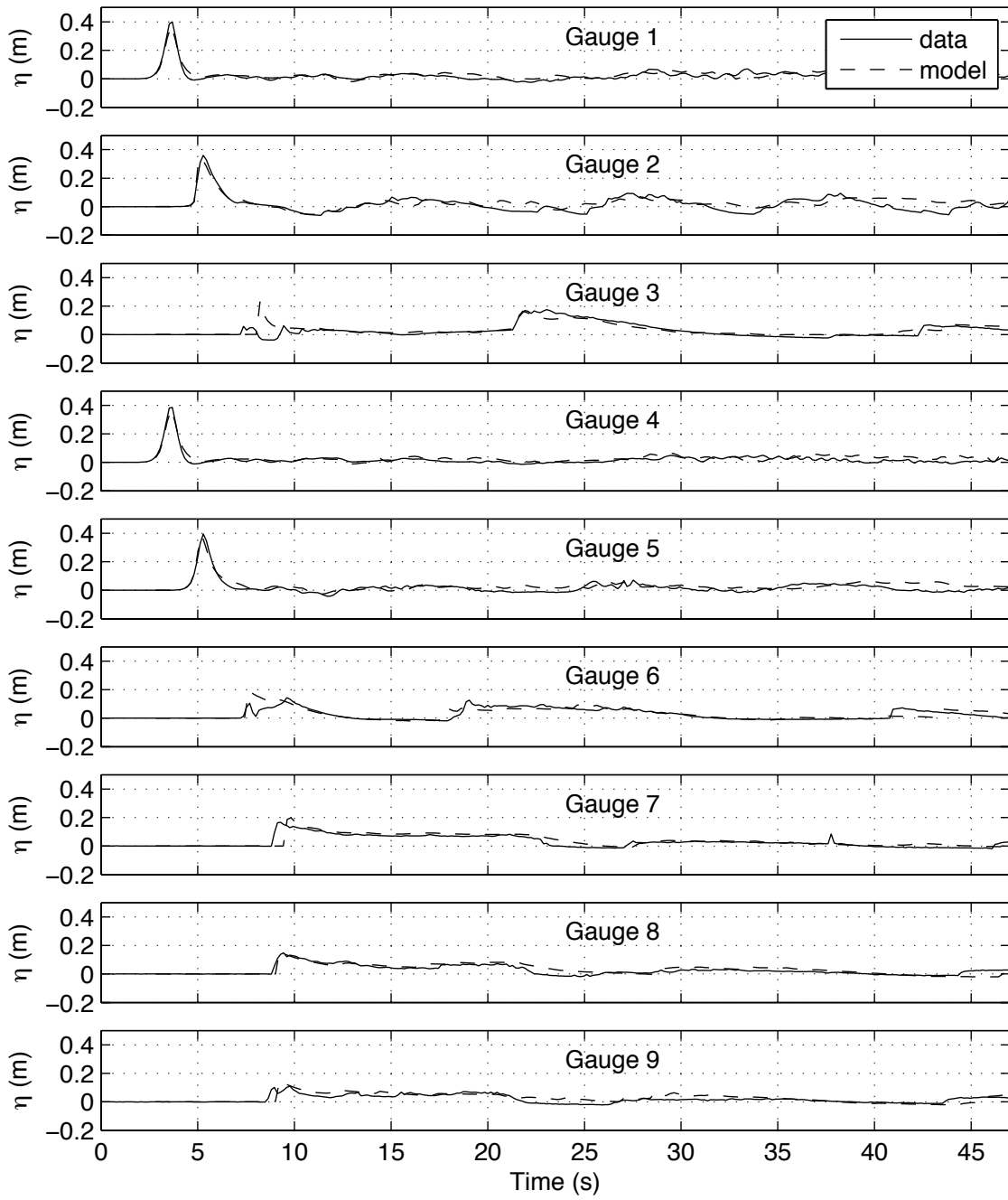


Figure 20: Model/data comparisons of time series of surface elevation at (top) Gauge 1 - Gauge 9. Solid line: model, stars: data.

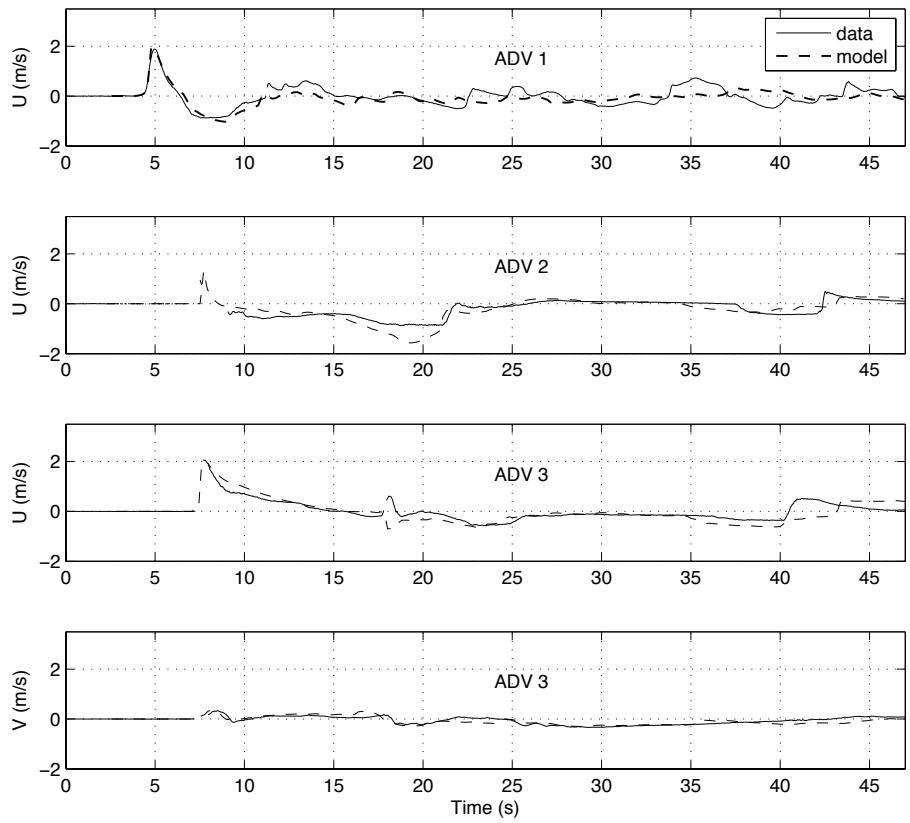


Figure 21: Model/data comparisons of time series of velocity  $u$  component at ADV 1 (top panel), ADV 2 (second panel), ADV 3 (third panel), and  $v$  component at ADV 3 (bottom panel). Solid line: model, dashed line: data.

time at both locations. An underprediction of the seaward velocity is found at ADV 2. The velocity in the  $y$ -direction was not compared at ADV 1 and ADV2 because the measured values were too small.

The input parameters for this test are listed below.

```
! -----DEPTH-----
DEPTH_TYPE = DATA
DEPTH_FILE = ../input/depth_wkshop.txt

! -----DIMENSION-----
Mglob = 501
Nglob = 261

! -----TIME-----
TOTAL_TIME = 45.0
PLOT_INTV = 0.2
PLOT_INTV_STATION = 0.2
SCREEN_INTV = 0.2

! -----GRID-----
DX = 0.1
DY = 0.1

! -----WAVEMAKER-----
WAVEMAKER = INI_SOL
AMP = 0.39
DEP = 0.78
LAGTIME = 5.0
XWAVEMAKER = 10.0 ! note that means  $x = 5$  m because the domain starts at  $x = -5$ 

! -----SPONGE LAYER-----
SPONGE_ON = F

! -----PHYSICS-----
DISPERSION = T
Gamma1 = 1.0
Gamma2 = 1.0
Gamma3 = 1.0
Beta_ref = -0.531
SWE_ETA_DEP = 0.80
Cd = 0.001
```

```

! -----NUMERICS-----
Time_Scheme = Runge_Kutta
HIGH_ORDER = FOURTH
CONSTRUCTION = HLLC
CFL = 0.5

! -----WET-DRY-----
MinDepth=0.001
MinDepthFrc = 0.001

! -----OUTPUT-----
DEPTH_OUT = T
U = T
V = T
ETA = T
MASK = T

```

Several post-processing procedures are performed in order to get model/data comparisons. First, *read\_result.m* is used to obtain time series of  $\eta$  at 9 pressure gauges, and  $u$  and  $v$  at 3 ADV locations. Then, *plot\_WG.m* is used for comparisons of surface elevation at the 9 gauges, *plot\_ADV\_AB.m* for comparisons of  $u$  at ADV 1 and 2, and *plot\_ADV\_C.m* for  $u$  and  $v$  at ADV 3.

## 5.6 Nesting case

We provide a 1-D example indicating that a solitary wave of permanent form is undistorted as it moves from a large domain Grid\_A to a smaller scale grid Grid\_B. In Grid\_A, the computational domain is 6000m long with 10 m constant water depth. Grid size is 4 m. An initial solitary wave with an amplitude of 1m is centered at  $x=1000.0$  m. Grid\_B, with a grid size of  $dx=2$ m, is nested inside Grid\_A. The nesting boundary is at  $x=2000.0$ m in Grid\_A. The calculation of Grid\_A provides a time series of  $u$ ,  $v$  and  $\eta$  through output at gauges at  $x=2000.0$ m ( $i = 500$ , where  $i$  is grid number in  $x$  direction in Grid\_A). The spherical mode is used as a demonstration of the nesting case.

There are three sub-directories for the nesting example.

**directory:** /examples/sph\_nesting /

/grid\_A/ contains input file, executive and station file for Grid\_A run.

/make\_nest\_file/ contains a Fortran code to generate the nesting input based on output from Grid\_A.

/grid\_B/ contains input file and executive file for Grid\_B calculation.

**procedure:**

1) run model Grid\_A. **NOTE:** the executive file should be compiled with '-DCOUPPLING' turned OFF (Makefile in /src/).

2) generate nesting input file using convert.f in /make\_nest\_file/.

3)run model Grid\_B. **NOTE:** the executive file should be compiled with '-DCOUPPLING' turned ON (Makefile in /src/).

**postprocessing:** use plot\_ab.m to plot results. Figure 22 shows results from Grid\_A (upper pannl) and Grid\_B (lower panel).

The input parameters for Grid\_A are listed below.

```
! -----DEPTH-----
DEPTH_TYPE = FLAT
DEPTH_FLAT = 10.0

! -----TIME-----
TOTAL_TIME = 400.0
PLOT_INTV = 1.0
PLOT_INTV_STATION = 0.0 ! 0.0 means make station output every time step for nesting data
SCREEN_INTV = 1.0

! -----GRID-----
StretchGrid = F
Lon_West = 120.0
Lat_South = 0.0
Dphi = 0.000035972
Dtheta = 0.0001

! -----WAVEMAKER-----
WAVEMAKER = INI_SOL
AMP = 0.1
DEP = 10.0
LAGTIME = 0.0
XWAVEMAKER = 1000.0

! -----PHYSICS-----
DISPERSION = T
Gamma1 = 1.0
Gamma2 = 0.0
Gamma3 = 1.0
Beta_ref=-0.531
```

SWE\_ETA\_DEP = 0.80  
Cd = 0.00

! -----NUMERICS-----  
Time\_Scheme = Runge\_Kutta  
HIGH\_ORDER = THIRD  
CONSTRUCTION = HLLC  
CFL = 0.5  
FroudeCap = 10.0

! -----OUTPUT-----  
NumberStations = 3  
STATIONS\_FILE = station.txt

The input parameters for Grid\_B are listed below.

! -----DEPTH-----  
DEPTH\_TYPE = FLAT  
DEPTH\_FLAT = 10.0

! -----TIME-----  
TOTAL\_TIME = 400.0  
PLOT\_INTV = 1.0  
PLOT\_INTV\_STATION = 1.00  
SCREEN\_INTV = 1.0

! -----GRID-----  
StretchGrid = F  
Lon\_West = 120.0  
Lat\_South = 0.0  
Dphi = 0.000017986  
Dtheta = 0.0001

! -----WAVEMAKER-----  
WAVEMAKER = INI\_SOL  
AMP = 0.1  
DEP = 10.0  
LAGTIME = 0.0  
XWAVEMAKER = 1000.0

! -----PHYSICS-----

DISPERSION = T  
Gamma1 = 1.0  
Gamma2 = 0.0  
Gamma3 = 1.0  
Beta\_ref=-0.531  
SWE\_ETA\_DEP = 0.80  
Cd = 0.00

! ————— NUMERICS —————  
Time\_Scheme = Runge\_Kutta  
HIGH\_ORDER = THIRD  
CONSTRUCTION = HLLC  
CFL = 0.5  
FroudeCap = 10.0

! ————— COUPLING —————  
COUPLING\_FILE = ../make\_nest\_file/coupling.txt

## References

- Agnon, Y., Madsen, P. A. and Schäffer, H. A., 1999, “A new approach to high-order Boussinesq models”, *J. Fluid Mech.*, **399**, 319-333.
- Berkhoff, J. C. W., Booy, N. and Radder, A. C., 1982, “Verification of numerical wave propagation models for simple harmonic linear water waves”, *Coast. Engrg.*, **6**, 255-279.
- Bermúdez, A. and Vázquez, M. E., 1994, “Upwind methods for hyperbolic conservation laws with source terms”, *Comput. Fluids*, **23** (8), 1049-1071.
- Briggs, M. J., Synolakis, C. E., and Harkins, G. S., 1994, “Tsunami run-up on a conical island”, *Proc., Waves-Physical and Numerical Modelling*, International Association for Hydraulic Research, Delft, The Netherlands, 446-455.
- Brown, J., MacMahan, J., Reniers, A. J. H. M. and Thornton, E., 2009, “Surf zone diffusivity on a rip-channeled beach”, *J. Geophys. Res.*, **114**, C11015, doi:10.1029/2008JC005158.
- Chen, Q., Dalrymple, R. A., Kirby, J. T., Kennedy, A. B. and Haller, M. C., 1999, “Boussinesq modelling of a rip current system”, *J. Geophys. Res.*, **104**, 20,617-20,637.
- Chen, Q., Kirby, J. T., Dalrymple, R. A., Kennedy, A. B. and Chawla, A., 2000, “Boussinesq modeling of wave transformation, breaking and runup. II: 2D”, *J. Waterway, Port, Coastal and Ocean Engineering*, **126**, 48-56.

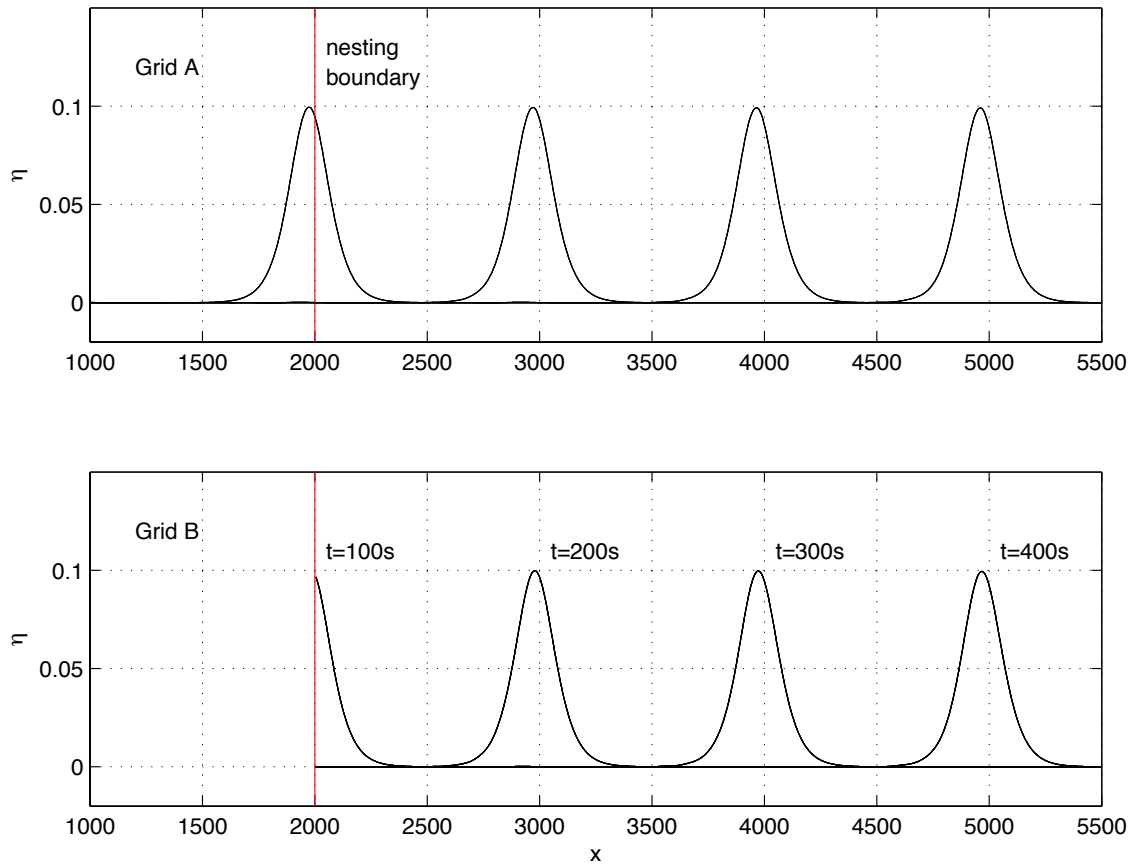


Figure 22: Solitary wave calculated in a larger domain Grid\_A (upper) and in a nested smaller domain Grid\_B (lower) at t=100s, 200s, 300s, and 400s.

- Chen, Q., Kirby, J. T., Dalrymple, R. A., Shi, F. and Thornton, E. B., 2003, "Boussinesq modeling of longshore currents", *Journal of Geophysical Research*, **108**(C11), 3362, doi:10.1029/2002JC001308.
- Chen, Q., Kaihatu, J. M., and Hwang, P. A., 2004, "Incorporation of Wind Effects Into Boussinesq Wave Models", *J. Waterway, Port, Coastal and Ocean Engineering*, **130**, 312-321.
- Chen, Q., 2006, "Fully nonlinear Boussinesq-type equations for waves and currents over porous beds", *Journal of Engineering Mechanics*. **132** (2): 220-230.
- Erduran, K. S., Ilic, S., and Kutija, V., 2005, "Hybrid finite-volume finite-difference scheme for the solution of Boussinesq equations", *Int. J. Numer. Meth. Fluid.*, **49**, 1213-1232.
- Gobbi, M. F., Kirby, J. T. and Wei, G., 2000, "A fully nonlinear Boussinesq model for surface waves. II. Extension to  $O(kh^4)$ ", *Journal of Fluid Mechanics*, **405**, pp. 181-210.
- Gottlieb, S., Shu C.-W., and Tadmor, E., 2001, "Strong stability-preserving high-order time discretization methods", *SIAM Review*, **43** (1), 89 - 112.
- Hansen, J. B., and Svendsen, I. A., 1979, "Regular waves in shoaling water: Experimental data", Tech. Rep. ISVA Ser., 21, Technical Univ. of Denmark, Denmark.
- Kennedy, A. B., Chen, Q., Kirby, J. T. and Dalrymple, R. A., 2000, "Boussinesq modeling of wave transformation, breaking and runup. I: 1D", *J. Waterway, Port, Coastal and Ocean Engineering*, **126**, 39-47.
- Kennedy, A. B., Kirby, J. T., Chen, Q. and Dalrymple, R. A., 2001, "Boussinesq-type equations with improved nonlinear performance", *Wave Motion*, **33**, pp. 225-243.
- Kim D. H., Cho, Y. S., and Kim, H. J., 2008, "Well-balanced scheme between flux and source terms for computation of shallow-water equations over irregular bathymetry", *Journal of Engineering Mechanics*, **134**, 277-290.
- Kim, D. H., Lynett, P. J. and Socolofsky, S. A., 2009, "A depth-integrated model for weakly dispersive, turbulent, and rotational fluid flows", *Ocean Modeling*, **27**, 198-214.
- Kim, D. H., 2009, "Turbulent flow and transport modeling by long waves and currents", Ph.D. dissertation, Texas A& M University.
- Kirby, J. T., Wei, G., Chen, Q., Kennedy, A. B. and Dalrymple, R. A., 1998, "FUNWAVE 1.0, Fully nonlinear Boussinesq wave model. Documentation and users manual". Report CACR-98-06, Center for Applied Coastal Research, Department of Civil and Environmental Engineering, University of Delaware.
- Kirby, J.T., Shi, F., Watts, P., Grilli, S.T., 2004, "Propagation of short, dispersive tsunami waves in ocean basins". EOS Transactions of the AGU 85 (47) Abstract OS21E-02.

- Kirby, J. T., Shi, F., Harris, J. C., and Grilli, S. T., 2012, "Sensitivity analysis of trans-oceanic tsunami propagation to dispersive and Coriolis effects", *Ocean Modelling*, under revision.
- Liang, Q. and Marche, F., 2009, "Numerical resolution of well-balanced shallow water equations with complex source terms", *Advances in Water Resources*, **32**, 873 - 884.
- Long, W. and Kirby, J. T., 2006, "Boussinesq modeling of waves, currents and sediment transport", Research Report No. CACR-06-02, Center for Applied Coastal Research, Dept. of Civil and Environmental Engineering, Univ. of Delaware, Newark.
- Lynett, P. J., Wu, T.-R. and Liu, P. L.-F., 2002, "Modeling wave runup with depth-integrated equations", *Coastal Engineering*, **46**, 89-107.
- Madsen, P.A., Srensen, O.R., 1992, "A new form of the Boussinesq equations with improved linear dispersion characteristics. Part 2. A slowly-varying bathymetry", *Coastal Engineering* **18** (3-4), 183-204.
- Mase, H., and Kirby, J. T., 1992, "Hybrid frequency-domain KdV equation for random wave transformation", *Proc., 23rd Int. Conf. Coast. Eng.*, ASCE, New York, 474-487.
- Naik, N. H., Naik, V. K., and Nicoules, M., 1993, "Parallelization of a class of implicit finite difference schemes in computational fluid dynamics", *International Journal of High Speed Computing*, **5**: 1-50.
- Ning, D. Z., Zang, J., Liang, Q., Taylor, P. H., and Borthwick, A. G. L., 2008, "Boussinesq cut-cell model for non-linear wave interaction with coastal structures", *International Journal for Numerical Methods in Fluids*, **57** (10), 1459-1483.
- Nwogu, O., 1993, "An alternative form of the Boussinesq equations for nearshore wave propagation", *Journal of Waterway, Port, Coastal, and Ocean Engineering*, **119** (6), pp. 618-638.
- Nwogu, O. and Demirbilek, Z., 2001, "BOUSS-2D: A Boussinesq wave model for coastal regions and harbors", ERDC/CHL TR-01-25, Coastal and Hydraulics Laboratory, USACOE Engineer Research and Development Center, Vicksburg, MS.
- Roeber, V., Cheung, K. F., and Kobayashi, M. H., 2010, "Shock-capturing Boussinesq-type model for nearshore wave processes", *Coastal Engineering*, **57**, 407-423.
- Rogers, B. D., Borthwick, A. G. L., and Taylor, P. H., 2003, "Mathematical balancing of flux gradient and source terms prior to using Roe's approximate Riemann solver", *Journal of Computational Physics*, **192**, 422-451.
- Shi, F., Kirby, J. T., Harris, J. C., Geiman, J. D., and Grilli, S. T., 2012 a, "A high-order adaptive time-stepping TVD solver for Boussinesq modeling of breaking waves and coastal inundation", *Ocean Modelling*, 43-44, 36-51.

- Shi, F., Kirby, J. T., and Tehranirad, B. , 2012 b, Tsunami benchmark results for spherical coordinate, Center for Applied Coastal Research Report, CACR 2012-02, University of Delaware, Newark, Delaware.
- Shi, F., Kirby, J. T., Tehranirad, B. and Harris, J. C., 2011, FUNWAVE-TVD, Version 1.0, users' manual and benchmark tests, Center for Applied Coastal Research Report, CACR 2011-04, University of Delaware, Newark, Delaware.
- Shi, F., Dalrymple, R. A., Kirby, J. T., Chen, Q. and Kennedy, A., 2001, "A fully nonlinear Boussinesq model in generalized curvilinear coordinates". *Coastal Engineering*, **42**, pp. 337-358.
- Shiach, J. B. and Mingham, C. G., 2009, "A temporally second-order accurate Godunov-type scheme for solving the extended Boussinesq equations", *Coastal Engineering*, **56**, 32-45.
- Sitanggang, K. I. and Lynett, P., 2005, "Parallel computation of a highly nonlinear Boussinesq equation model through domain decomposition", *Int. J. Num. Meth. Fluids*, **49**, 57-74.
- Smagorinsky, J., 1963, "General circulation experiments with the primitive equations. I. The basic experiment", *Mon. Weather Rev*, **91**, 99-165.
- Swigler, D. and Lynett, P. ,2011, "Laboratory study of the three-dimensional turbulence and kinematic properties associated with a solitary wave traveling over an alongshore-variable, shallow shelf", in review.
- Synolakis, C. E., Bernard, E. N., Titov, V. V., Kânoglu, U. and González, F. I., 2007, "Standards, criteria, and procedures for NOAA evaluation of tsunami numerical models", *NOAA Tech. Memo. OAR PMEL-135*, National Oceanic and Atmospheric Administration.
- Tehranirad, B., Shi, F., Kirby, J. T., Harris, J. C. and Grilli, S., 2011, "Tsunami benchmark results for fully nonlinear Boussinesq wave model FUNWAVE-TVD, Version 1.0", Research Report No. CACR-11-02, Center for Applied Coastal Research, University of Delaware.
- Tehranirad, B., Shi, F., Kirby, J. T., Harris, J. C. and Grilli, S., 2013, "Tsunami benchmark results for fully nonlinear Boussinesq wave model FUNWAVE-TVD, Version 2.1", Research Report No. CACR-13-10, Center for Applied Coastal Research, University of Delaware.
- Tehranirad, B., Shi, F. and Kirby, J. T. , 2012 b, Tsunami benchmark results for spherical coordinate, Center for Applied Coastal Research Report, CACR 2013-10, University of Delaware, Newark, Delaware.
- Ting, F.C.K., Kirby, J.T., 1994, "Observation of undertow and turbulence in a laboratory surf zone". *Coast. Eng.* **24**, 5180.
- Tonelli, M. and Petti, M., 2009, "Hybrid finite volume - finite difference scheme for 2DH improved Boussinesq equations", *Coast. Engrng.*, **56**, 609-620.

- Tonelli, M. and Petti, M., 2010, "Finite volume scheme for the solution of 2D extended Boussinesq equations in the surf zone", *Ocean Engrng.*, **37**, 567-582.
- Toro, E. F., 2009, *Riemann solvers and numerical methods for fluid dynamics: a practical introduction*, Third edition, Springer, New York.
- Wei, G., Kirby, J.T., Grilli, S.T., Subramanya, R., 1995, "A fully nonlinear Boussinesq model for surface waves: Part I. Highly nonlinear unsteady waves", *Journal of Fluid Mechanics* **294**, 7192.
- Wei, G. and Kirby, J. T., 1995, "A time-dependent numerical code for extended Boussinesq equations", *Journal of Waterway, Port, Coastal and Ocean Engineering*, **120**, pp. 251-261.
- Yamamoto, S., Daiguji, H., 1993, "Higher-order-accurate upwind schemes for solving the compressible Euler and NavierStokes equations", *Computers and Fluids*, **22** (2/3), 259270.
- Yamamoto, S., Kano, S. and Daiguji, H, 1998, "An efficient CFD approach for simulating unsteady hypersonic shockshock interference flows", *Computers and Fluids*, **27** (56), pp. 571-580.
- Zelt, J. A., 1991, "The runup of nonbreaking and breaking solitary waves", *Coastal Engineering*, **15**, pp. 205-246.
- Zhen, F., 2004, "On the numerical properties of staggered vs. non-staggered grid schemes for a Boussinesq equation model", MCE Thesis, Department of Civil and Environmental Engineering, University of Delaware.
- Zhou, J. G., Causon, D. M., Mingham C. G., and Ingram, D. M., 2001, "The surface gradient method for the treatment of source terms in the shallow-water equations", *Journal of Computational Physics*, **168**, 1-25.